Nanosized drug delivery systems based on polyion complex vesicles (PICsomes) pioneered by developing novel encapsulation methods

後藤, 晃範

Nanosized drug delivery systems based on polyion complex vesicles (PICsomes) pioneered by developing novel encapsulation methods

(ポリイオンコンプレックス型ベシクル(PICsomes)への新規物質内封法が開拓するナノ薬物送達システムに関する研究)

Akinori Goto

Table of Contents

Chapter I. General introduction

I.1. Nano-sized particle for DDS

The key objective of drug delivery system (DDS) technology is to deliver an effective amount of a drug to affected parts of the body. Other benefits of DDS include improved absorption, improved pharmacokinetics, improved drug stability, sustained release (reduced administration frequency), and fewer side effects. In particular, drugs with potent effects, such as anticancer drugs, should be administered via a DDS owing to the severe side effects that can occur when they exert their systemic effects.

Various DDS have been explored and developed, and as technology has advanced, submicron/nano-sized dosage forms have been developed. As shown in Figure I-1, dendrimers, liposomes, micelles, and polymers are representative nano-sized DDS. The discovery of the enhanced permeation and retention (EPR) effect led to the development of nano-sized DDS. Normal vascular tissue is closely packed and hinders the permeation of particles larger than 20 nm. Vascular permeability is markedly enhanced owing to the rapid growth of vascular tissue in the tumor periphery, and particles smaller than approximately 200 nm can pass through the vessels. Accordingly, particles ranging between 20 and 200 nm are more likely to accumulate in the tumor vicinity. Moreover, because the lymphatic system is underdeveloped around the tumor, accumulated particles cannot be excreted and tend to accumulate around the tumor (Figure I-2). This is called the EPR effect [I-1,I-2], which has served as the basic theory for the development of nano-sized DDS. In recent years, particles sized ~100 nm can reach the surrounding tumor, tend to accumulate in the stroma, and are less likely to be taken up by cancer cells. In contrast, particles ~30 nm in size are easily taken up by cancer cells beyond the stroma [I-3]. The mechanism of leakage from blood vessels was visually captured, in which nanoparticles exit from a portion of the blood vessel as if erupting, called nano-eruption [I-4]. In general, nano-sized particles are relatively easily taken up by cells. For example, particles sized 100 nm were six times more likely to be taken up by Caco-2 cells than particles sized 1 μm during cellular uptake experiments [I-5]. Using the rat intestinal loop model, it was found that 100-nm-sized particles are 15 to 250 times more likely to be taken up in cells than 1- or 10-μm-sized particles [I-6]. Hence, a nano-sized DDS is an interesting formulation, and size is considered the most fundamental parameter governing the pharmacokinetics of cancer DDS.

Recently, vesicle-type DDSs have attracted considerable attention. Vesicle-type DDSs have an aqueous phase and can contain hydrophilic compounds. Liposomes have been extensively investigated in vesicle-type DDS, and 14 products were approved by the Food and Drug Administration (FDA) by 2022, including the first FDA-approved doxorubicin-loaded PEGylated liposome (Doxil®) [I-7], vincristine-loaded liposome (Marqibo®) and irinotecan-loaded liposome (Onivyde®) [I-8]. Liposomes comprise a lipid bilayer membrane that retains hydrophobic compounds, improving the stability, pharmacokinetics, cellular uptake, and metabolism of the encapsulated compounds. Given that liposomes are excreted by macrophages, covering the membrane surface with

polyethylene glycol (PEG) ensures stealth and prevents phagocytosis by macrophages [I-9]. Another vesicle-type DDS is the polymersome, which exhibits similar characteristics to the liposome [I-10–I-13]. Polymersomes, comprising polymers, are interesting vesicles owing to their unique properties, such as membrane tunability, ability to load hydrophilic compounds, including anticancer drugs, semipermeable membranes, and self-assembly [I-10–I-13]. Typically, polymersomes are formed from a block copolymer consisting of hydrophilic and hydrophobic portions [I-10–I-13]. Additionally, polymersomes can be formed from graft copolymers and branched copolymers [I-14,I-15]. These polymers are chemically synthesized, allowing for a high degree of design flexibility. PEG is the major hydrophilic polymer used to prepare an amphiphilic block-copolymer, which affords polymersomes biocompatible and stealth properties, similar to liposomes. Several methods have been developed to prepare polymersomes via self-assembly. The preparation methods were classified into two groups: solvent-switching and polymer rehydration. In the solvent-switching method, the block polymer is dissolved in an organic solvent, which is then slowly hydrated to make the hydrophobic part insoluble and increase the interfacial tension between the hydrophobic part and water to induce vesicle formation. The size of the obtained vesicles varied depending on the organic solvent used. In polymer rehydration, block polymers are dissolved in an organic solvent. A thin film was then prepared by evaporating the solution. Subsequently, the thin film is hydrated by the addition of water, followed by the expansion of polymer layers and the formation of bulges due to the hydration force, finally forming polymersomes [I-16]. Preparation methods that do not require organic solvents have also been developed [I-11]. Furthermore, polymersomes exhibit disadvantages in terms of *in vivo* stability and control of the release behavior of retained drugs. Polyion-complex vesicles (PICsomes) have been developed to overcome these disadvantages.

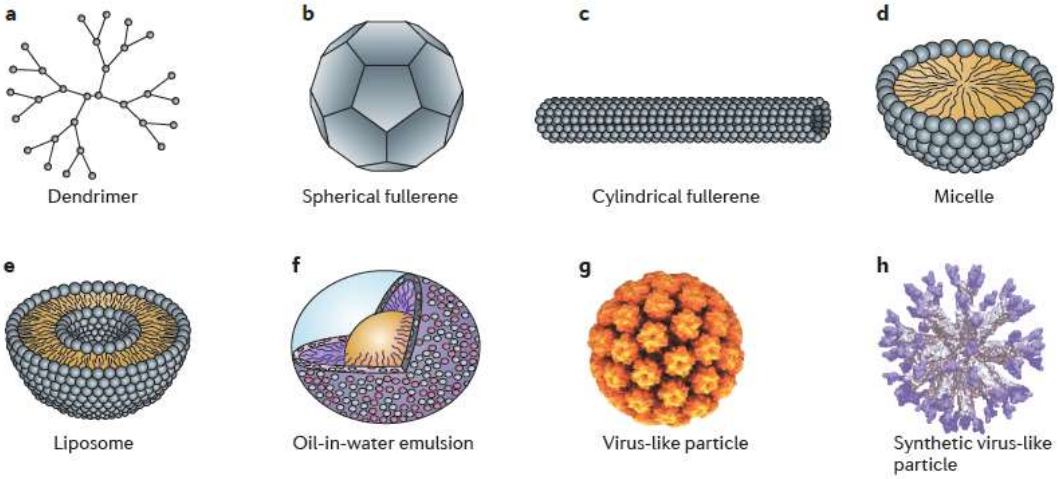

i

Size	<5 nm	10–20 nm	50–100 nm	>150 nm
Nanoparticle	Dendrimer	Polymer	DNA polyplex	Liposome
Bioactivity	Partition like small molecules and filter through the kidney	Escape the vasculature, infiltrate the tissues and lymphatics like proteins	Penetrate the mucosal membranes and the skin and are taken up into cells.	Taken up mainly into phagocytic cells

Figure I-1. Examples of nanotechnology-based drug carriers. Nanotechnologies that can be applied to immunoregulation include nanoparticles (parts a–c), nanoemulsions (parts d–f) and virus-like particles (parts g–h). Nanoparticles include dendrimers which branch out (part a), carbon molecules known as spherical fullerenes (part b) and cylindrical carbon molecules known as cylindrical fullerenes (part c). Nanoemulsions incorporate immiscible components such as oil and water that might form amphiphilic molecules such as micelles (part d), liposomes with a lipid bilayer (part e) and oil-in-water emulsions (part f). Virus-like particles are self-assembled structures composed of one or more viral capsid proteins (part g), whereas synthetic virus-like particles are self-assembled from chemically synthesized components (part h). Examples of the relationship between nanoparticle size and bioactivity are shown in (part i). [I-17].

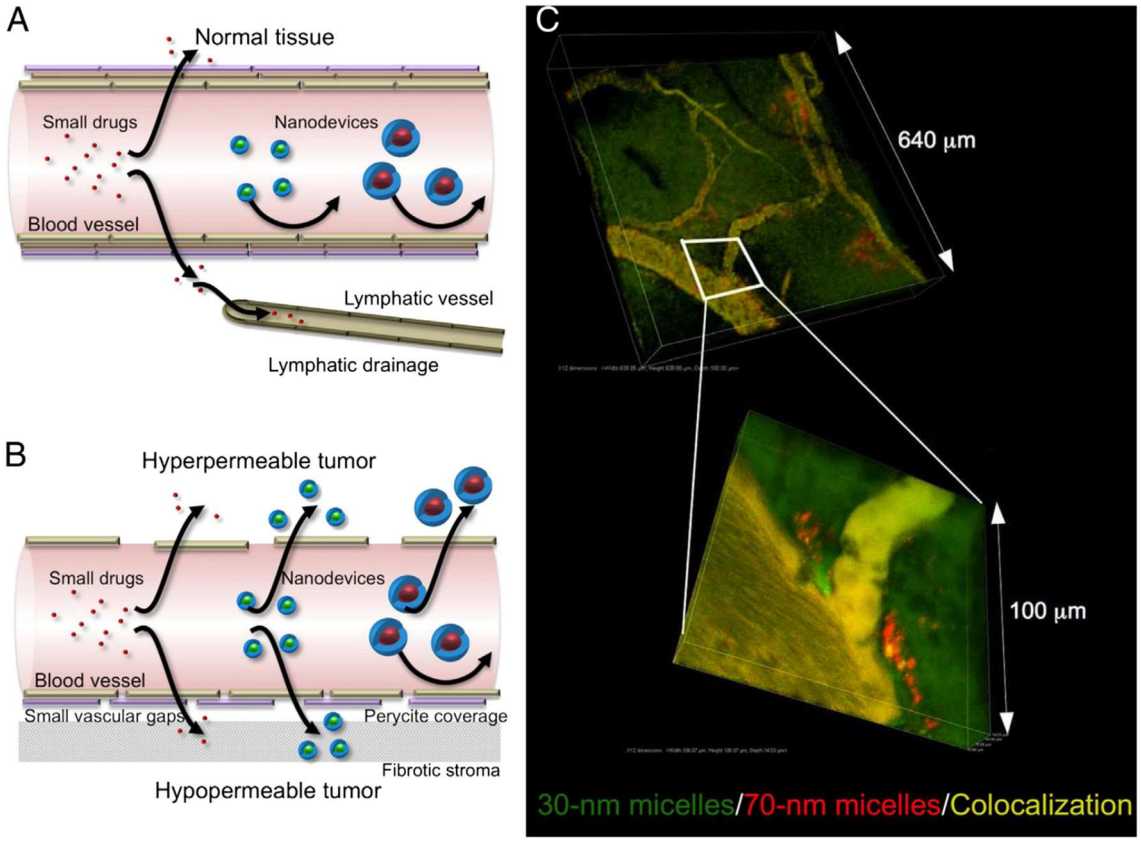

Figure I-2. A. Small drugs can diffuse, penetrate and be cleared by lymphatics in normal tissues, while nanodevices are restricted to the vascular compartment due to the continuous endothelium. B. Endothelial cells of tumor neovasculature present large fenestrations, allowing nanodevices to extravasate extensively in tumor tissues. Moreover, these nanodevices are retained due to slow venous return and poor lymphatic clearance. In tumors with poor permeability, the extravasation and penetration of large nanodevices may be impaired by nanopathophysiological parameters such as small fenestrations, pericyte coverage of the vasculature and fibrotic stroma. C. The extravasation and penetration of 1,2-diaminocyclohexane) platinum (II) (DACHPt)-loaded polymeric micelles in poorly permeable pancreatic tumors depended on their size. Micelles with 30-nm diameter were labeled with Alexa-488 (green) and micelles with 70-nm were labeled with Alexa-594 (red). Colocalization is observed as yellow [I-18].

I.2. Polyion complex vesicles (PICsomes)

As shown in Figure I-3, PICsomes are formed from a homo-polycation, PEG_{2000}-poly([5-aminopentyl]-α,β-aspartamide)$_X$ (PEG-P(Asp-AP)), and a block-polyanion, PEG_{2000}-poly(α,β-aspartic acid)$_Y$ (PEG-P(Asp)). Because these polymers comprise amino acids, they show low toxicity risk when decomposed *in vivo* [I-19]. Major features of the PICsomes include: 1) a hollow vesicle capable of self-assembly in aqueous solution, which can be easily prepared without the use of organic solvents; 2) the carboxylic acid and amino groups in the polymer that form the membrane can be crosslinked using a crosslinking agent; 3) a tunable size; 4) a semipermeable membrane, with the possibility of encapsulating nanoparticles and water-soluble macromolecules in the inner aqueous phase; 5) excellent blood circulation and tumor accumulation properties; and 6) functional properties. The following section provides an overview of these characteristics.

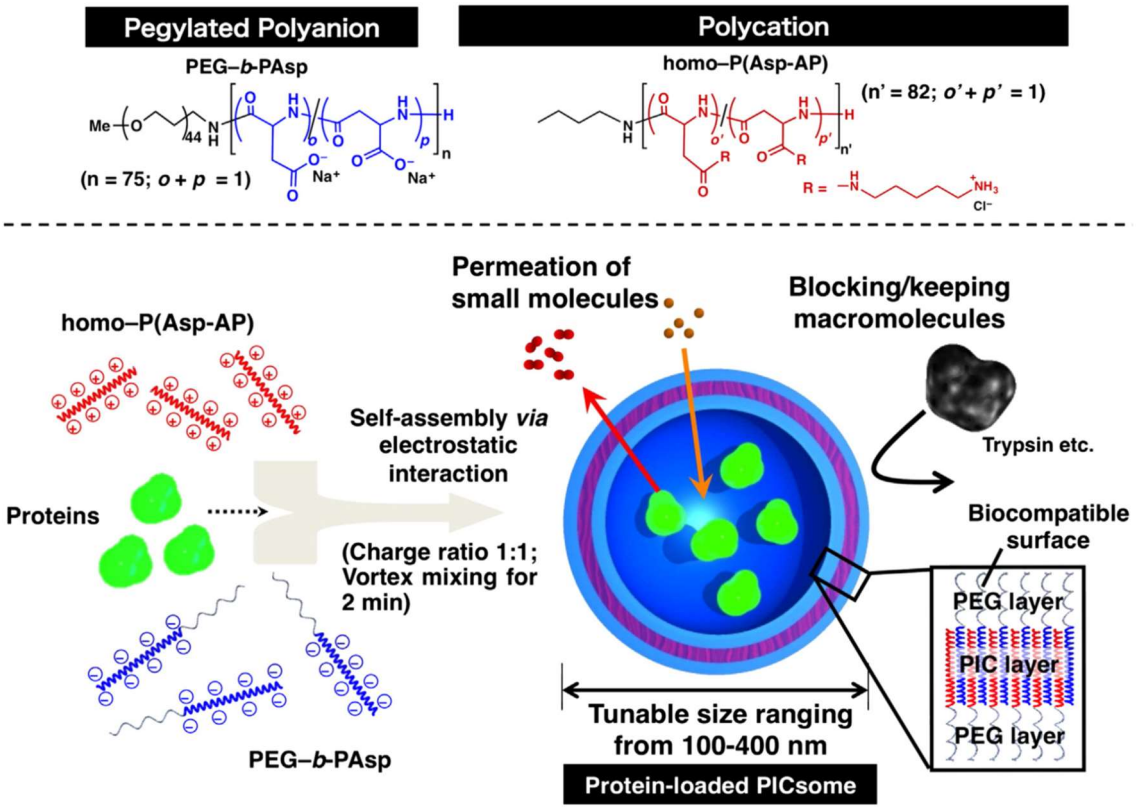

Figure I-3 Schematic representation of preparation and characteristics of PICsomes. (Top) Chemical structures of polyelectrolytes for Nano-PICsome formation. (Bottom) Schematic representation of preparation of Nano-PICsomes and semipermeability of PICsomes [I-18].

I.2.1. Self-assembly in aqueous solutions

Each polymer used for PICsome preparation was dissolved in phosphate buffer, respectively. Each solution was then mixed at a 1:1 stoichiometric ratio of carboxylic acid to amino functions. No organic solvents are used to prepare PICsomes, and the risk of residual solvents when administered *in vivo* is low [I-19]. Both polymers assemble and form PIC via electrostatic interactions, with phase separation from the aqueous solution. The use of block copolymers with uncharged hydrophilic chains, PEG, allows structural control at the nanoscale level. One example of a hollow-structured vesicle is PICsomes, in which PICs have a monolayer lamellar structure sandwiched between PEG layers. For vesicle formation, the PEG content should be less than 10% of the vesicle weight [I-20]. The formation of a pair of units, called unit PICs (u-PICs), whose charges nearly cancel each other, can be observed. u-PICs self-assemble to form nanostructures [I-20]. Interestingly, un-crosslinked PICsomes increased in size after incorporating the surrounding u-PICs (Figure I-4). The presence of salts, such as NaCl, in an aqueous solution can impact the formation of u-PICs and their further assembly, resulting in changes in the size of PICsomes, the formation of other structures without PICsomes, and the absence of PIC assembly [I-21].

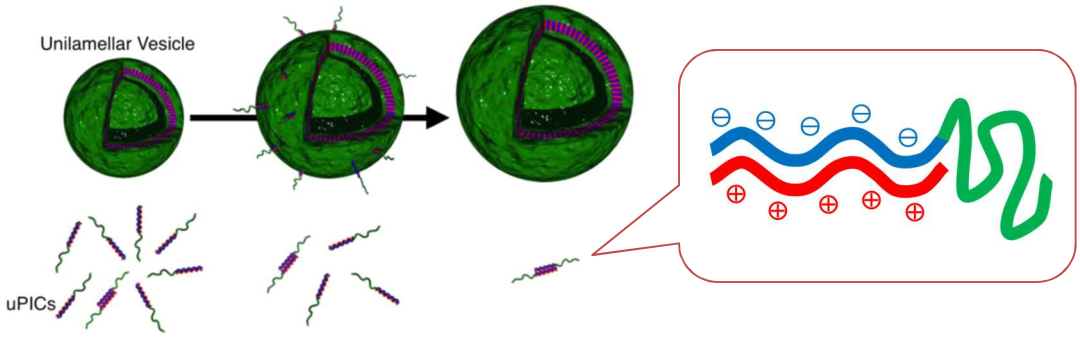

Figure I-4 The proposed mechanism of growth of nano-PICsomes. Adapted with permission from [I-20]. Copyright 2013 American Chemical Society

I.2.2. Stabilization by crosslinking

PICsomes are composed of homo-polycations containing amino groups and blocked polyanions containing carboxyl groups. The PIC membrane is stabilized by crosslinking using condensing agents, such as EDC, to create amide bonds. Un-crosslinked PICsomes are unstable in 10 mM phosphate-buffered saline (PBS; 150 mM NaCl). However, crosslinked PICsomes are stable in 10 mM PBS without changing their size, and crosslinked PICsomes are stable *in vivo* [I-18]. Crosslinking using glutaraldehyde has also been reported [I-22].

I.2.3. Tunable size

PICsomes can be tuned to sizes ranging from 100 to 400 nm by varying the polymer concentration in the aqueous solution during vesicle formation (Table I-1). Micelles with an average particle size of ~40 nm were formed using cationic and anionic polymers modified with PEG. In contrast, substituting PEG-P(Asp) for homo-P(Asp) resulted in the formation of monodisperse hollow particles with an average diameter of >100 nm. The average size of the produced particles increased with increasing polymer concentration, and the particle size distribution extended slightly, forming monodisperse hollow vesicles [I-19].

Table I-1 DLS analysis of PIC assemblies prepared from different combinations at various concentrations. Reprinted with permission from [I-19]. Copyright 2010 American Chemical Society

combination of polymers	Concentration (mg/mL)	size (mean ± (SEM[a])[b] (nm)	polydispersity index
PEG-P(Asp)/PEG-P(Asp-AP)	1	39.0 ± 1.10	0.051 ± 0.011
PEG-P(Asp)/Homo-P(Asp-AP)	0.1	100 ± 1.60	0.041 ± 0.012
	0.5	99.3 ± 3.20	0.048 ± 0.012
	1	100 ± 1.40	0.023 ± 0.016
	2	155 ± 3.70	0.037 ± 0.012
	3	218 ± 11.9	0.041 ± 0.014
	4	244 ± 14.3	0.042 ± 0.010
	5	310 ± 12.5	0.051 ± 0.015
	7	344 ± 16.3	0.078 ± 0.010
	10	387 ± 21.7	0.078 ± 0.013

a: Standard error of the mean (SEM) (n = 3). b:Each value was calculated using the cumulant method.

I.2.4. Semipermeable membrane and encapsulating water-soluble polymers or nanoparticles

Given the presence of an internal cavity, PICsomes can encapsulate and deliver water-soluble polymers and inorganic nanoparticles into their inner aqueous phase. The membranes forming PICsomes are semipermeable. For example, using PEG-P(Asp)$_{100}$/PEG-P(Asp-AP)$_{100}$, fluorescein isothiocyanate-dextran (FITC-Dex; molecular weight, ~40,000) can be stably encapsulated into PICsomes for as long as 3 months. Moreover, tetramethylrhodamine isothiocyanate-dextran (TRITC-Dex; molecular weight, ~70,000) was encapsulated in the PICsomes; however, TRITC with a molecular weight of ~443.5 could easily bypass the PIC membrane and leak out [I-23]. Recently,

membrane crosslinking was found to not only stabilize PICsomes but also impact their semipermeability. PICsomes with a low degree of crosslinking can permeate larger molecules, and compounds with a molecular weight of ≤6000 can pass through the PIC membrane regardless of the degree of crosslinking [I-24].

Because the PIC membrane is semipermeable, it can encapsulate water-soluble polymers and nanoparticles such as enzymes. For example, as shown in Figure I-5, enzymes such as β-galactosidase and L-asparaginase can be encapsulated in PICsomes, and enzyme-encapsulated PICsomes can function as nanoreactors that convert small-molecular weight substrates supplied from outside the PICsome and then released outside [I-25,I-26]. PICsomes encapsulated in carboxyl dextran-coated superparamagnetic iron oxide (SPIO) enable tumor tracking using magnetic resonance imaging (MRI) [I-27]. Accordingly, it is possible to encapsulate water-soluble polymers in the PICsomes owing to the semipermeable membrane, while water-soluble low molecular weight compounds (WLMWCs) with molecular weights below 1000 are small-molecule drugs.

Two methods for encapsulating water-soluble polymers into PICsomes have been developed: 1) mixing polycation, polyanion, and the material to be encapsulated and then forming PICsomes [I-23], and 2) mixing the material to be encapsulated and un-crosslinked PICsomes, which are broken into u-PICs by physical stimulation, and then reforming the PICsomes [I-25,I-26]. However, these methods are unsuitable for encapsulating charged substances because they interfere with the formation of u-PICs. Moreover, the payload amount depends on the concentration during the encapsulation process. A higher concentration of the material to be encapsulated during the encapsulation process leads to a larger amount of encapsulation. However, the physical properties of the solution containing the encapsulated material may inhibit PICsome formation. Thus, the encapsulation of PICsomes is currently limited.

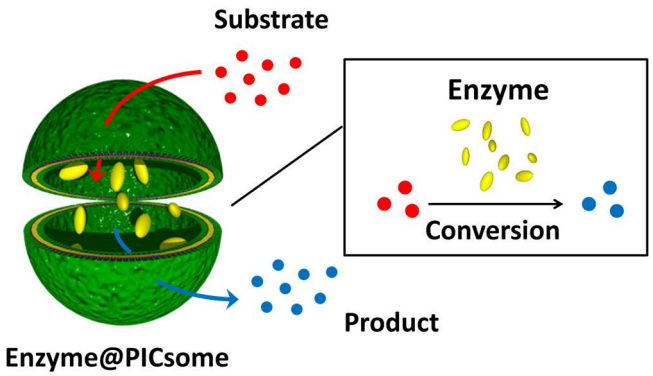

Figure I-5 Schematic illustration of enzyme-loaded PICsome (enzyme@PICsome) system.

I.2.5. Prolonged blood circulation and good tumor accumulation

The prolonged blood retention of PICsomes was sufficient for the EPR effect and resulted in good tumor accumulation. For solid tumor targeting, PICsomes ~100 nm in size effectively accumulate in tumors (C26), whereas PICsomes >150 nm show poor tumor accumulation as they become larger [I-28].

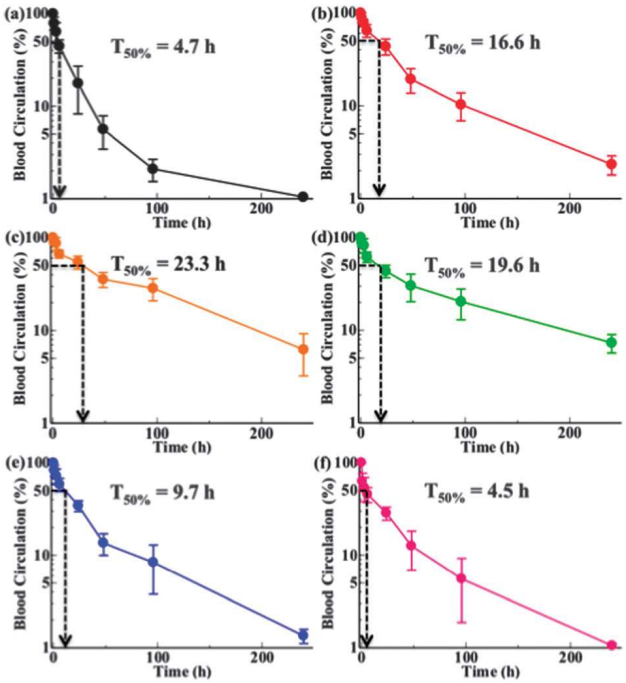

Figure I-6 Blood circulation profile of Cy5-PIC micelles and cross-linked Cy5-Nano-PICsomes: PIC-38 (a), PIC-102 (b), PIC-158 (c), PIC-197 (d), PIC-256 (e), PIC-298 (f) (n = 3). Dashed lines show the time corresponding to the removal of 50% of injected dose ($T_{50\%}$) [I-28]. Copyright 2011 ROYAL SOCIETY OF CHEMISTRY.

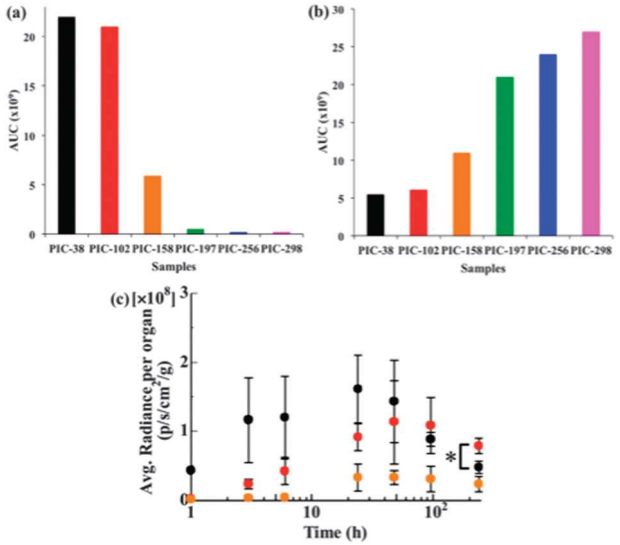

Figure I-7 Area under the curves (AUC) of cross-linked Cy5-Nano-PICsomes (red: PIC-102, orange: PIC-158, green: PIC-197, blue: PIC-256, pink: PIC-298) and PIC micelles (black: PIC-38) in selected organs (a: C-26 tumor, b: spleen). (c) Time profile of tumor accumulation (black: PIC-38, red: PIC-102, orange: PIC-158) evaluated by fluorescence imaging (n = 3). * $P < 0.05$. [I-28]. Copyright 2011 ROYAL SOCIETY OF CHEMISTRY.

I.2.6. Addition of new functions

The potential of PICsomes as DDS can be enhanced by chemically modifying the PICsome-comprising polymer with a suitable ligand for targeting. The uptake of PICsomes modified with cRGD, which is specifically recognized by $\alpha_V\beta_3$ and $\alpha_V\beta_5$ integrins abundantly expressed on neovascularity, was increased into human umbilical vein endothelial cells. The 40% cRGD-modified PICsomes showed the highest accumulation in the tumor neovasculature [I-29]. This technology could be applied in therapeutic and diagnostic methods by enabling delivery to sites where ligand-free PICsomes are difficult to deliver.

Other examples of functionalization have been reported, such as environmentally responsible PICsomes, responses to pH, salt intensity, and temperature [I-30–I-34].

I.3. The purpose of this study

To develop a DDS platform, the carrier must 1) be applicable to as many types of compounds as possible, 2) be stable even in harsh environments, such as *in vivo*, 3) have targeting ability for therapeutic purposes, 4) possess a release profile exhibiting appropriate pharmacological effects, and 5) have low (no) toxicity. The objective of the current study was to enhance the utility of PICsomes by developing an efficient method for encapsulating WLMWCs and enzymes.

For PICsomes, which are expected to be next-generation DDS platforms, it is important for issue 1) to be able to deliver WLMWCs to the lesion, as described in Chapter I.2.4. Certain small-molecule drugs exhibit excellent efficacy but are difficult to use owing to their side effects and metabolic issues. DDS can substantially contribute to drug therapy by reducing side effects while acting at the required site. To address this problem, in Chapters II and IV, I examined the utilization of the space within the PICsome to load WLMWCs. Another concept is the use of enzyme prodrug therapy (EPT), given that PICsomes have suitable physical properties for use in EPT. If enzyme-encapsulated PICsomes can be delivered selectively to the lesion, the prodrug can be converted to an active form locally (in the lesion), and therapy can be continued until the loss of enzyme activity. Furthermore, the side effects can be reduced by controlling the biodistribution of PICsomes. Therefore, it is necessary to prepare enzyme-encapsulating PICsomes that maintain sufficient enzymatic activity. In Chapter III, I describe the development of a method for preparing enzyme-encapsulated PICsomes that afford higher enzyme activity than conventional preparation methods by utilizing the characteristics of PIC membranes. I evaluated the *in vitro* and *in vivo* functionalities of the enzyme-encapsulated PICsomes obtained using this method.

I.4. References

I-1. Hiroshi Maeda, Minoru Ueda, Tetsuo Morinaga, and Tomonori Matsumoto. Conjugation of poly(styrene-comaleic acid) derivatives to the antitumor protein neocarzinostatin: pronounced improvements in pharmacological properties. *J. Med. Chem.* **1985**, 28, 455–461.

I-2. H. Maeda, J. Takeshita, R. Kanamaru. A lipophilic derivative of neocarzinostatin. A polymer conjugation of an antitumor protein antibiotic. *Int. J. Pept. Protein Res.***1979**, 14, 81–87.

I-3. H. Cabral, Y. Matsumoto, K. Mizuno, Q. Chen, M. Murakami, M. Kimura, Y. Terada, M. R. Kano, K. Miyazono, M. Uesaka, N. Nishiyama, K. Kataoka. Accumulation of sub-100 nm polymeric micelles in poorly permeable tumours depends on size. *Nat. Nanotech.* **2011**, 6, 815-823.

I-4. Yu Matsumoto, Joseph W. Nichols, Kazuko Toh, Takahiro Nomoto, Horacio Cabral, Yutaka Miura, R. James Christie, Naoki Yamada, Tadayoshi Ogura, Mitsunobu R. Kano, Yasuhiro Matsumura, Nobuhiro Nishiyama, Tatsuya Yamasoba, You Han Bae, Kazunori Kataoka. Vascular bursts enhance permeability of tumour blood vessels and improve nanoparticle delivery. *Nat. Nanotech.* **2016**, 11, 533-538.

I-5. M.P. Desai, V. Labhasetwar, E. Walter, R.J. Levy, G.L. Amidon. The mechanism of uptake of biodegradable microparticles in Caco-2 cells is size dependent. *Pharm. Res.* **1997**, 14, 1568–1573.

I-6. M.P. Desai, V. Labhasetwar, G.L. Amidon, R.J. Levy. Gastrointestinal uptake of biodegradable microparticles: effect of particle size. *Pharm. Res.* **1996**, 13, 1838–1845.

I-7. Yechezkel (Chezy) Barenholz. Doxil® — The first FDA-approved nano-drug: Lessons learned. *J. Control Release* **2012**;160, 117–34.

I-8. Peng Liu, Guiliang Chen and Jingchen Zhang. A Review of Liposomes as a Drug Delivery System: Current Status of Approved Products, Regulatory Environments, and Future Perspectives. *Molecules* **2022**, 27, 1372.

I-9. Alexander L. Klibanovl, Kazuo Maruyamal, Vladimir P. Torchilin and Leaf Huang. Amphipathic polyethyleneglycols effectively prolong the circulation time of liposomes. *FEBS. letters* **1990**, 268, 235-237.

I-10. Fatemeh Araste, Ali Aliabadi, Khalil Abnous, Seyed Mohammad Taghdisi, Mohammad Ramezani, Mona Alibolandi. Self-assembled polymeric vesicles: Focus on polymersomes in cancer treatment. *J. Controlled Release* **2021**, 330, 502–528.

I-11. Maliheh Hasannia, Ali Aliabadi, Khalil Abnous, Seyed Mohammad Taghdisi, Mohammad Ramezani, Mona Alibolandi. Synthesis of block copolymers used in polymersome fabrication: Application in drug delivery. *J. Controlled Release* **2022**, 341, 95–117.

I-12. Rohini Kotha, Divya Dhatri Kara, Rajeshwari Roychowdhury, Katikala Tanvi, Mahalaxmi Rathnanand. Polymersomes Based Versatile Nanoplatforms for Controlled Drug Delivery and Imaging. *Adv. Pharm. Bull.* **2023**, 13(2), 218-232.

I-13. P. Peter Ghoroghchian, Guizhi Li, Dalia H. Levine, Kevin P. Davis, Frank S. Bates, Daniel A. Hammer, and Michael J. Therien. Bioresorbable Vesicles Formed through Spontaneous Self-Assembly of Amphiphilic Poly(ethylene oxide)-blockpolycaprolactone. *Macromolecules* **2006**, 39, 1673–1675.

I-14. Hyun Jin Lee, Seung Rim Yang, Eun Jung An, Jong-Duk Kim. Biodegradable Polymersomes from Poly(2-hydroxyethyl aspartamide) Grafted with Lactic Acid Oligomers in Aqueous Solution. *Macromolecules* **2006**, 39, 4938–4940.

I-15. Zengqian Shi, Yongfeng Zhou, Deyue Yan. Facile Fabrication of pH-Responsive andSize-Controllable Polymer Vesicles Froma Commercially Available Hyperbranched Polyester. *Macromol. Rapid Commun*. **2008**, 29, 412–418.

I-16. Jung Seok Lee, Jan Feijen. Polymersomes for drug delivery: Design, formation and characterization. *J. Controlled Release* **2012**, 161, 473–483.

I-17. Douglas M. Smith, Jakub K. Simon and James R. Baker Jr. Applications of nanotechnology for immunology. *Nat. Rev. Immunol.* **2013**, 13, 592–605.

I-18. Horacio Cabral, Kanjiro Miyata, Akihiro Kishimura. Nanodevices for studying nano-pathophysiology. *Adv. Drug Delivery Rev.* **2014**, 74, 35–52.

I-19. Yasutaka Anraku, Akihiro Kishimura, Makoto Oba, Yuichi Yamasaki, Kazunori Kataoka. Spontaneous formation of nanosized unilamellar polyion complex vesicles with tunable size and properties. *J. Am. Chem. Soc*. **2010**, 132, 1631–1636.

I-20. Yasutaka Anraku, Akihiro Kishimura, Yuichi Yamasaki, Kazunori Kataoka. Living Unimodal Growth of Polyion Complex Vesicles via Two-Dimensional Supramolecular Polymerization. *J. Am.*

Chem. Soc **2013**, 135, 1423−1429.

I-21. Sayan Chuanoi, Akihiro Kishimura, Wen-Fei Dong, Yasutaka Anraku, Yuichi Yamasaki, Kazunori Kataoka. Structural factors directing nanosized polyion complex vesicles (Nano-PICsomes) to form a pair of block aniomer/homo catiomers: studies on the aniomer segment length and the catiomer side-chain structure. *Polym. J.* **2014**, 46, 130–135.

I-22. Beob Soo Kim, Sayan Chuanoi, Tomoya Suma, Yasutaka Anraku, Kotaro Hayashi, Mitsuru Naito, Hyun Jin Kim, Ick Chan Kwon, Kanjiro Miyata, Akihiro Kishimura and Kazunori Kataoka. Self-Assembly of siRNA/PEG-b-Catiomer at Integer Molar Ratio into 100 nm-Sized Vesicular Polyion Complexes (siRNAsomes) for RNAi and Codelivery of Cargo Macromolecules. *J. Am. Chem. Soc*. **2019**, 141, 3699−3709.

I-23. Aya Koide, Akihiro Kishimura, Kensuke Osada, Woo-Dong Jang, Yuichi Yamasaki, Kazunori Kataoka. Semipermeable Polymer Vesicle (PICsome) Self-Assembled in Aqueous Medium from a Pair of Oppositely Charged Block Copolymers: Physiologically Stable Micro-/Nanocontainers of Water-Soluble Macromolecules. *J. Am. Chem. Soc.* **2006**, 128, 5988-5989.

I-24. Omer F. Mutaf, Yasutaka Anraku, Akihiro Kishimura, Kazunori Kataoka. Unilamellar polyion complex vesicles (PICsomes) with tunable permeabilities for macromolecular solutes with different shapes and sizes. *Polymer* **2017**, 133, 1-7.

I-25. Yasutaka Anraku, Akihiro Kishimura, Mako Kamiya, Sayaka Tanaka, Takahiro Nomoto, Kazuko Toh, Yu Matsumoto, Shigeto Fukushima, Daiki Sueyoshi, Mitsunobu R. Kano, Yasuteru Urano, Nobuhiro Nishiyama, Kazunori Kataoka. Systemically Injectable Enzyme-Loaded Polyion Complex Vesicles as In Vivo Nanoreactors Functioning in Tumors. *Angew. Chem. Int. Ed*. **2016**, 55, 560–565.

I-26. Daiki Sueyoshi, Yasutaka Anraku, Toru Komatsu, Yasuteru Urano, Kazunori Kataoka. Enzyme-Loaded Polyion Complex Vesicles as in Vivo Nanoreactors Working Sustainably under the Blood Circulation: Characterization and Functional Evaluation. *Biomacromolecules*. **2017**, 18, 1189−1196.

I-27. Daisuke Kokuryo, Yasutaka Anraku, Akihiro Kishimura, Sayaka Tanaka, Mitsunobu R. Kano, Jeff Kershaw, Nobuhiro Nishiyama, Tsuneo Saga, Ichio Aoki, Kazunori Kataoka. SPIO-PICsome: Development of a highly sensitive and stealth-capable MRI nano-agent for tumor detection using SPIO-loaded unilamellar polyion complex vesicles (PICsomes). *J. Controlled Release* **2013**, 169, 220–227.

I-28. Yasutaka Anraku, Akihiro Kishimura, Atsushi Kobayashi, Makoto Oba, Kazunori Kataoka. eSize-controlled long-circulating PICsome as a ruler to measure critical cut-off disposition size into normal and tumor tissues. *Chem. Commun*. **2011**, 47, 6054–6056.

I-29. Wataru Kawamura, Yutaka Miura, Daisuke Kokuryo, Kazuko Toh, Naoki Yamada, Takahiro Nomoto, Yu Matsumoto, Daiki Sueyoshi, Xueying Liu, Ichio Aoki, Mitsunobu R Kano, Nobuhiro

Nishiyama, Tsuneo Saga, Akihiro Kishimura, Kazunori Kataoka. Density-tunable conjugation of cyclic RGD ligands with polyion complex vesicles for the neovascular imaging of orthotopic glioblastomas. *Sci. Technol. Adv. Mater*. **2015**, 16, 035004.

I-30. Akihiro Kishimura, Sittipong Liamsuwan, Hiroyuki Matsuda, Wen-Fei Dong, Kensuke Osada, Yuichi Yamasaki and Kazunori Kataoka. pH-dependent permeability change and reversible structural transition of PEGylated polyion complex vesicles (PICsomes) in aqueous media. *Soft Matter* **2009**, 5, 529-532.

I-31. Yuki Ohara, Keita Nakai, Sana Ahmed, Kazuaki Matsumura, Kazuhiko Ishihara and Shin-ichi Yusa. pH-Responsive Polyion Complex Vesicle with Polyphosphobetaine Shells. *Langmuir* **2019**, 35(5), 1249–1256.

I-32. Sayan Chuanoi, Yasutaka Anraku, Mao Hori, Akihiro Kishimura, and Kazunori Kataoka. Fabrication of Polyion Complex Vesicles with Enhanced Salt and Temperature Resistance and Their Potential Applications as Enzymatic Nanoreactors. *Biomacromolecules* **2014**, 15(7), 2389–2397.

I-33. Junjie Li, Yasutaka Anraku and Kazunori Kataoka. Self-Boosting Catalytic Nanoreactors Integrated with Triggerable Crosslinking Membrane Networks for Initiation of Immunogenic Cell Death by Pyroptosis. *Angew. Chem. Int. Ed*. **2020**, 59, 13526–13530.

I-34. Beob Soo Kim, Mitsuru Naito, Rimpei Kamegawa, Hyun Jin Kim, Ryo Iizuka, Takashi Funatsu, Shingo Ueno, Takanori Ichiki, Akihiro Kishimura and Kanjiro Miyata. Photo-reactive oligodeoxynucleotide-embedded nanovesicles (PROsomes) with switchable stability for efficient cellular uptake and gene knockdown. *Chem. Commun*. **2020**, 56, 9477–9480.

Chapter II. MSN@PICsome for sustained release of WLMWCs

II.1. Introduction

To develop PICsomes as a next-generation DDS platform, it is necessary to load several modalities. Given that PICsomes are vesicles comprising a semipermeable membrane, it is not possible to load water-soluble low-molecular-weight compounds (WLMWCs) into the internal aqueous phase (Chapter I.2.4). Therefore, we encapsulated an inorganic matrix to load WLMWCs into the inner space.

Mesoporous silica is an inorganic material used as an adsorbent in several studies. The size of mesoporous silica can be easily tuned, allowing the preparation of mesoporous silica nanoparticles (MSN). The porous structure of the silica particles provides a markedly large surface area in relation to their diameter, allowing greater adsorption than silica particles of the same size. Furthermore, silica is easily surface-modified, and the WLMWC amount adsorbed can be increased by introducing functional groups on the silica surface to meet this purpose [II-1–II-7]. Moreover, unsintered silica has low cytotoxicity because it is easily degraded in the *in vivo* environment [II-8,II-9]. Thus, MSNs are considered the best inorganic material for loading WLMWCs into PICsomes.

In the current study, I developed a modified method for encapsulating MSNs in PICsomes and prepared MSN-encapsulated PICsomes (MSN@PICsomes). Furthermore, the MSN surface in the PICsome was modified to alter the loading and release behavior of WLMWCs, and the therapeutic effects of WLMWCs were evaluated *in vitro* and *in vivo*. 2',2'-Difluoro-2'-deoxycytidine (gemcitabine, GEM) was selected as a model drug because GEM is widely used as an anticancer drug, and its cytotoxic effect has been demonstrated. However, when administered intravenously, GEM is quickly metabolized to an inactive form in the blood, liver, and kidneys, resulting in higher doses and stronger side effects. Therefore, a suitable DDS formulation is required [II-10–II-13].

II.2. Material and Methods

II.2.1. Material characterization

A Zetasizer-nano (Malvern Instruments Ltd., Worcestershire, UK) was used to measure particle size by Dynamic light scattering (DLS). A Mobius (Wyatt Technology Corporation, Santa Barbara, CA, USA) was used for measuring zetapotential. Transmission electron micrographs (TEM) were obtained using a JEM-1400 transmission electron microscope (JEOL Ltd., Tokyo, Japan) operating at 120 kV. The samples for TEM observation were dispersed in purified water, and transferred onto copper grids (400 mesh size; coated with a thin film of collodion and carbon), followed by staining with uranyl acetate. For TEM observation of cross-sectioned specimens, the sample was purified and concentrated by centrifugal ultrafiltration, followed by fixing with 2% osmic acid solution, embedded in an epoxy resin (EPON 812), and cut with a Sorvall Porter-Blum MT-2 ultramicrotome to a thickness of ca. 50 nm. The ultrathin section was transferred onto a Cu mesh grid, and stained with uranyl acetate for 10 min and lead citrate for 2 min, and dried at RT. Energy-dispersive

X-ray spectroscopy (EDS) analysis was performed using a JEM-2100 transmission electron microscope (JEOL Ltd.) operating at 200 kV with a JED-2100T detector (JEOL Ltd.). UV−visible spectra were obtained on a Nanodrop ND-1000 (Thermo Fisher Scientific Inc.). Absorbance of microplate samples was measured using a Microplate Instrumentation AD200 (Beckman Coulter Inc., Brea, CA, USA). Fluorescence intensity was measured using an FP-6600 fluorescence spectrophotometer (JASCO Corporation, Tokyo, Japan). Energy dispersive X-ray spectrometry fluorescence spectrometry (EDS-FS) analysis (XGT-5200WR, Horiba Ltd., Kyoto, Japan) was used for the evaluation of sulfonate modification of MSN.

II.2.2. Synthesis of MSN

MSN was prepared as reported previously [II-6]. Typically, 0.15 g of cetyltrimethylammonium bromide (CTAB) was dissolved in 50 mL of warm distilled water, followed by adjusting of the solution pH to ca. 12 with sodium hydroxide solution. Then, 0.4 mL of tetraethyl orthosilicate (TEOS) was added to the CTAB solution at 70 °C and vigorously stirred at ca. 300 rpm for 5 min. Subsequently, 3 mL of ethyl acetate was added, and the mixture was stirred for 3 h, resulting in a whitish solution. The resulting mixture was cooled down to room temperature while stirring. Subsequently, the solution was centrifuged at 12,000 × *g* for 60 min, and the supernatant was removed. Twenty milliliters of ethanol was added to the residue, followed by dispersion by ultrasonication. The pH of the resulting dispersion was adjusted to *ca.* 1 using hydrochloric acid, and then heated at 60°C for 3 h while stirring to remove CTAB. The obtained reaction mixture was centrifuged at 12 000 × *g* for 60 min, and the supernatant was then removed. The residue was washed 3 times with ethanol, and completely dried under reduced pressure at 40°C, to give MSN (0.086 g).

II.2.3. Preparation of MSN@PICsome

Poly(5-aminopentyl-α,β-aspartamide) (P(Asp-AP), with a degree of polymerization (DP) of 82) and polyethylene glycol (PEG)-blockpoly(α,β-aspartic acid) (PEG−PAsp, DP of PAsp = 75; Mn of PEG = 2 000, Mw/Mn of PEG = 1.05), were prepared as reported previously [II-14]. P(Asp-AP) and PEG−PAsp were separately dissolved in 10 mM phosphate buffer (PB; pH7.4) at a final concentration of 1 mg/mL. The MSN was dispersed in 10 mM PB (pH7.4) at a final concentration of 10 mg/mL. Fivehundred forty microliters of the P(Asp-AP) solution was mixed with 18.8 μL of the MSN colloidal solution, and the mixture was subjected to vortex mixing for 2 min and then allowed to stand for 8 min. Then, 400 μL of the PEG−PAsp solution was added to this mixture, followed by vortex mixing for 2 min; this mixture contained the same residual molar concentration of −NH3 + from P(Asp-AP) and −COO− from PEG−PAsp. The weight ratio of MSN to total polymer was 1:5. Next, 550 μL of 10 mg/mL EDC solution was added to the reaction mixture, and stood overnight at

room temperature to cross-link the PIC layer for further purification and all the other experiments. The resulting solution was purified using a poly(ether sulfone) (PES) ultrafiltration membrane (molecular weight cutoff (MWCO): 300 000) at 25 °C. The medium exchange was repeated 10 times to completely remove byproducts from the solution to obtain the sample termed MSN*@ PICsome, composed of MSN-encapsulated PICsome, empty PICsome, and free MSN.

II.2.4. Evaluation of Efficacy of MSN Loading into PICsome.

The efficacy of MSN loading, which is defined by a ratio of the amount of MSN encapsulated in the PICsome to the amount of feed MSN, was determined by capillary electrophoresis (CE), performed on a model P/ACE MDQ CE apparatus (Beckman Coulter, Inc.) equipped with a 75 μm capillary (TSP075375, Molex). Electrolyte was 200 mM glycine buffer (pH 8.0). Applied voltage for separation was set to 5 kV. Two samples, i.e., a solution of MSN*@PICsome and a physical mixture of empty PICsome and free MSN, were prepared for analysis. The MSN*@PICsome was dispersed at a total polymer concentration of 0.7 mg/mL. As a control, the mixture solution of free MSN and empty PICsome in a weight ratio of 1:5 was prepared with adjusting the total polymer concentration to 0.7 mg/mL. Both MSN*@PICsome and free MSN were labeled with FITC through adsorption onto the silica surface of the MSN to allow fluorescence detection. One milliliter of the MSN*@PICsome and the free MSN solutions were treated with 10 μL of 5 mg/mL ethanol solution of FITC for the labeling. This solution was then purified by ultrafiltration using PES ultrafiltration membrane (MWCO: 300 000) until excess FITC was removed.

II.2.5. Surface Modification of MSN

Free MSN fraction was removed from the MSN*@PICsome sample using an Oasis MAX column (Waters corporation, Milford, MA, USA) before modification. Hereafter, the obtained purified sample in this way was termed MSN@PICsome. Surface modifications of MSN were carried out using silane coupling agents. Typical methods are detailed below.

II.2.5.1. Introduction of Amino Groups.

Cross-linked MSN@PICsome containing 2 mg of MSN was dispersed in 5 mL of purified water. Then, 3-Aminoproplytriethoxysilane (APTS) was added in a dropwise manner to the solution as 1% per water volume, and stirred overnight at room temperature. The product was collected by ultrafiltration using a PES ultrafiltration membrane (MWCO: 300 000) at 25 °C, and washed 10 times with purified water to completely remove unreacted APTS from the solution. The resulting solution contained amino-functionalized MSN@PICsome (A-MSN@PICsome). Bare amino-functionalized

MSN (A-MSN) was prepared similarly, but was purified by washing with water 5 times to completely remove unreacted APTS. Introduced amount of amino groups was determined by spectrophotometric analysis based on TNBS assay using empty PICsome as a reference.

II.2.5.2. Introduction of Sulfonate Groups

Cross-linked MSN@PICsome containing 2 mg of MSN was dispersed in 5 mL of 1% acetic acid. Then, 3-mercaptoproplytriethoxysilane (MPTS) was added in a dropwise manner to the solution up to a 1% per volume, and stirred overnight at room temperature. The product was collected by ultrafiltration using a PES ultrafiltration membrane (MWCO: 300 000) at 25 °C, and washed 5 times with 1% acetic acid, and another 5 times with purified water, to completely remove unreacted MPTS from the solution. Subsequently, the collected mercapto-MSN@PICsome was dispersed in 5 mL of purified water, followed by mixing with 5 μL of concentrated sulfuric acid and 100 μL of 30% hydrogen peroxide for oxidation of mercapto-groups to sulfonate-groups. The reaction mixture was stirred overnight at room temperature. The resulting solution was neutralized using sodium hydroxide. The product was collected by ultrafiltration using a PES ultrafiltration membrane (MWCO: 300 000) at 25 °C, and washed 10 times with purified water, to completely remove salt. The resulting solution contained sulfonate-functionalized MSN@PICsome (S-MSN@PICsome). Bare sulfonate-functionalized MSN (S-MSN) was prepared similarly, except for the purification process as follows: Bare mercapto-MSN was centrifuged and washed with 1% acetic acid 5 times to completely remove unreacted MPTS. After the sulfonation, S-MSN was centrifuged and washed with water 5 times to completely remove salt.

II.2.6. Drug Absorption and Release Test

MSN@PICsome (without any modification), A-MSN@PICsome, and S-MSN@PICsome were used for absorption and release of drugs. These solutions were prepared using 10 mM phosphate-buffered saline (PBS; 10 mM PB with 150 mM NaCl, pH7.4) at 2 mg/mL of MSN. For absorption of RoseBengal (RB), 5 mL of each solution (containing 10 mg of MSN) was added to 20 mL of RB solution (2.0 mg/mL) separately, and allowed to stand overnight. Then, the PICsome was removed using a PES ultrafiltration membrane (MWCO: 300 000) at 25 °C, and the collected solutions were analyzed by absorption spectrophotometry at a fixed wavelength of 550 nm to determine the residual amount of RB in the solution. The absorption amount was calculated as the difference between the initial and residual RB concentration.

Absorption tests of Gemcitabine (GEM) were performed similarly. Solutions of MSN@PICsome, A-MSN@PICsome, and S-MSN@PICsome were prepared using 10 mM PBS (pH7.4) at 2 mg/mL of MSN. Ten milliliters of each solution (containing 20 mg of MSN) was added

to 20 mL of GEM solution (1.5 mg/mL), separately, and allowed to stand overnight. Each formulation was washed to remove excess GEM by ultrafiltration. Then, the collected filtrates were analyzed by absorption spectrophotometry to determine the residual amount of GEM in the solution. Purification was repeated until GEM was not detected in the filtrate. The absorption amount was calculated as the difference between the initial and residual GEM concentration. For release test of GEM, 2 mL of the resulting solution of GEM-absorbed S-MSN@PICsome (GEM-S-MSN@PICsome) was placed into a dialysis bag, and release test was performed at 37 °C using 20 mL of 10 mM PBS (pH7.4) or simulated body fluid (SBF, pH7.4) as an outer solution. SBF (pH 7.4) contains Na^+, K^+, Mg^{2+}, Ca^{2+}, Cl^-, $HCO3^-$, $HPO4^{2-}$, and $SO4^{2-}$ at the same level as human body. GEM concentration was determined by absorption spectrophotometry using a fixed wavelength of 270 nm (n = 3).

II.2.7. Evaluation of Cytotoxicity

To evaluate cytotoxicity, I seeded C26 or A549 cells in 96-well plates (2.2 × 103 cells/well) and preincubated for 24 h at 37 °C under a humidified atmosphere of 5% CO2. Six preparations, viz., GEM-S-MSN@PICsome, GEM, S-MSN@PICsome, GEM-S-MSN, S-MSN, and empty PICsome were used for cytotoxicity evaluation as solutions in 10 mM PBS (pH 7.4), as listed in Table S2. The final GEM concentration of GEM-S-MSN@PICsome, GEM, and GEM-S-MSN was 0.1 μg/mL for A549 cells, and 0.5 μg/mL for C26 cells. Concentration of MSN contained in SMSN@ PICsome and S-MSN were adjusted to that of GEM-S-MSN@PICsome and GEM-S-MSN, respectively. The cells were exposed to each of the 6 preparations for 48 or 72 h, followed by analysis using cell counting kit-8 (Dojindo Molecular Technologies, Inc.), involving incubation for 1 h at 37 °C. To prepare a blank and a negative control sample, 10 mM PBS (pH 7.4) and the cell culture medium were added to the cells. Finally, the absorbance was measured at 450 nm using a Microplate Instrumentation plate reader.

II.2.8. Blood Retention of MSN and MSN*@PICsome.

For fluorescence labeling of MSN, Cy5 was adsorbed onto the silica surface of the MSN. To obtain Cy5-labeled MSN*@PICsome, 5 mg of Cy5 was added to 1 mL of the MSN*@PICsome solution containing 4 mg of the MSN, and stood overnight. The product was washed by 10 mM PBS (pH7.4) 20 times using a PES ultrafiltration membrane (MWCO: 300 000) at 25 °C to remove the residual Cy5. Cy5-labeled MSN was prepared by the same method using the MSN instead of the MSN*@PICsome. Cy5-labeled empty PICsome was prepared using Cy5-conjugated PEG−PAsp (PEG−PAsp−Cy5) instead of nonlabelled PEG−PAsp, as previously reported [II-14].

Two hundred microliters of solutions of the Cy5-labeled MSN*@PICsome (1 mg/mL as PEG−PAsp), the Cy5-labeled MSN (the same MSN concentration to the Cy5-labeled

MSN*@PICsome), and the Cy5-labeled empty PICsome (1 mg/mL as PEG−PAsp−Cy5) in 10 mM PBS (pH 7.4) were systemically administered, respectively, into BALB/c mice by tail vein injection. Mice were sacrificed 1 h after the administration, and blood was collected from the postcaval vein using heparinized syringe. After centrifugation of the collected blood at 12 000 × *g* for 5 min at 4°C, fluorescence of the resulting supernatant was measured (Ex/Em = 650/670 nm). As a positive control, each sample solution was diluted 10-fold by mouse plasma. All measurements were repeated 3 times for each sample.

II.2.9. Evaluation of In Vivo Therapeutic Efficacy and Biodistribution of GEM-MSN@PICsome.

Each BALB/c nude mouse was subcutaneously inoculated with 50 μL of a suspension of A549 cells in RPMI-1640 with 10% Fetal Bovine Serum (FBS, 3×10^7 cells/mL). Tumors were allowed to grow for 14 days (Average tumor volume is 8.7 mm^3). GEM-S-MSN@PICsome, S-MSN@PICsome, GEM-SMSN, S-MSN, PICsome, GEM, and 10 mM PBS (pH7.4) were prepared for administration as described above. Twohundred microliters of each solution were injected into the tail vein of mice. The dose of GEM was 5 mg/kg, and formulations without GEM were administered at a concentration equivalent to the polymers or MSN included in 5 mg/kg GEM-S-MSN@PICsome. Each formulation was administered 3 times with a 7-day interval (days 0, 7, and 14 days). Tumor size was measured twice a week using a digital vernier caliper across both perpendicular diameters, and its volume, V, was calculated using the following formula

$$V = (a^2 b) / 2$$

where a and b are the minor and major diameter of the tumor.

For the biodistribution study, A549-tumor bearing mice (BALB/c nude, female; 5 weeks old; n = 5) were prepared as above. GEM-SMSN@PICsome and PICsome (a negative control) were prepared using Cy5-labeled polymer instead of nonlabeled polymer [II-14]. Polymer concentration was adjusted to the same concentration with the in vivo therapeutic experiment. GEM-S-MSN was prepared as follows: Cy5 was added to the S-MSN dispersed solution for fluorescence labeling. The resulting solution was purified using a PES ultrafiltration membrane (MWCO: 300 000) at 25 °C. The PBS buffer (pH7.4) was exchanged repeatedly until excess Cy5 was removed completely from the sample to obtain Cy5-loaded S-MSN. Then, GEM was absorbed in Cy5-loaded S-MSN similarly. MSN concentration was adjusted to contain the same amount of MSN with GEM-S-MSN@PICsome. Two-hundred microliters of 10 mM PBS solutions of each formulation were injected into the tail vein of mice. As a positive control of plasma clearance evaluations, each sample solution was diluted 10-fold by mouse plasma. Blood was collected from the postcaval vein using heparinized syringes, and

the main organs (lung, kidney, liver, and spleen) and A549 tumor tissues were excised. After centrifugation of the collected blood at 12 000 × *g* for 5 min at 4 °C, fluorescence of the resulting supernatant was measured using a plate reader. The main organs and tumor tissues were homogenized using 5 × Passive Lysis Buffer (Promega, Tokyo, Japan), and the resulting colloidal solutions were analyzed by spectrofluorometry using a microplate reader (Ex/Em = 643/667 nm).

II.3. Results and discussion

II.3.1. Synthesis of MSN

The size of synthesized MSNs was a monodisperse (polydispersity index (PdI): 0.09) with an average diameter of about 70 nm. TEM images showed that the MSNs had a spherical and mesoporous structure (Figure II-1). MSN showed negative charge, −18.1 mV, because of the silanol groups on the surface. Thus, the obtained MSNs had a suitable size for encapsulation in PICsomes and for drug delivery applications.

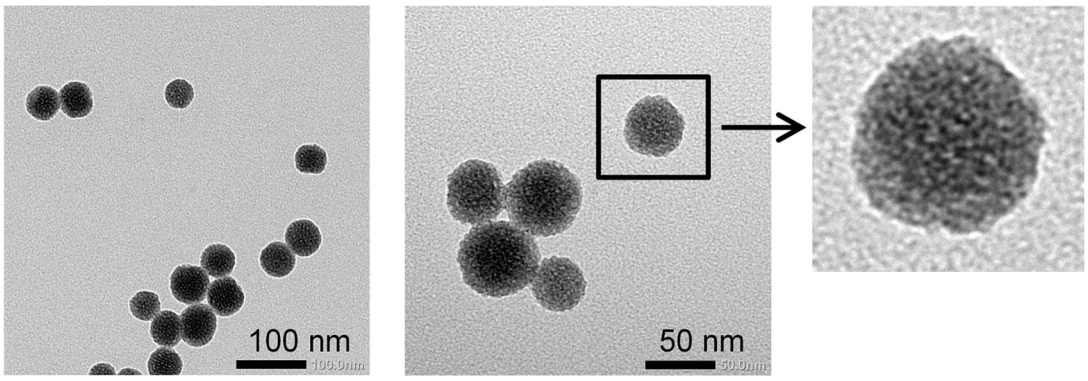

Figure II-1 TEM images of synthesized MSN.

II.3.2. Preparation of MSN@PICsome

According to the mechanism of PICsome formation, charged substances can interact with the oppositely charged polymers that composed the PICsome and inhibit vesicle formation during at loading process [II-15,II-16]. MSN has a negative charge and can cause this problem. In fact, PEG-PAsp, P(Asp-AP), and MSN was mixed directly, visible aggregates were formed and no monodisperse PICsomes were formed (data not shown). To improve this issue, positively charged P(Asp-AP) was added to MSN followed by negatively charged PEG-PAsp (Figure II-2). The products were then cross-linked to increase stability and purified, MSN*@PICsome was obtained. The resulting MSN*@PICsome had an average size of 105 nm and PdI of 0.15. The average zeta potential in 10 mM PBS (pH 7.4) was −2.8 mV, which was significantly neutral value than the −18.1 mV observed for MSN. TEM images of MSN*@PICsome revealed the presence of two types of particles with

different contrasts, with the darker contrast particles considered to be MSN-encapsulated PICsome (Figure II-3a). Few unencapsulated MSNs were observed, and Many PICsomes (low contrast particles) that did not encapsulate MSNs were present. The number ratio of high contrast PICsome particles estimated based on TEM images was about 30% (Table II-1). Cross-sectional TEM images confirmed that MSN particles, seen as high-contrast spherical particles (indicated by arrows in Figure II-3b), were encapsulated in PICsome. This result indicates that MSNs are encapsulated into PICsomes, which was also confirmed by EDS analysis (Figure II-4). The strong Si signal from free MSN was observed and visualized clearly. On the other hand, MSN@PICsome, a particle with strong contrast in the bright-field image, also showed a Si signal. However, it was weaker than that of free MSN. This result suggests that MSNs are covered by the PIC membrane. The empty PICsome, which was only visualized in the brightfield image, had a Si signal intensity similar to that of the background.

Prepared samples, MSN*@PICsomes labeled with FITC and the mixture of MSN and PICsome, were analyzed by CE to estimate the efficacy of MSN loading. Three major peaks were found in the electropherogram of the MSN*@PICsome solution (indicated by arrows in Figure II-5). In this CE measurement condition, eluting time should be correlated with the net negative charge of analytes. The averaged zeta potentials of MSN, MSN@PICsome and empty PICsome in 10 mM PBS (pH7.4) were −18.1, −2.8 and −0.3 mV, respectively. Accordingly, peak (1), which eluted at about 3 min, was assigned to MSN@PICsome having only a slightly negative zeta potential. Peaks (2) and (3) were assigned to free-FITC and bare MSN, respectively, by comparing to the result obtained for a physical mixture of FITC-labeled MSN and non-labeled PICsome shown in Figure II-5b. Here, no peak was observed at the elution time of ca. 3 min, indicating negligible physical interaction of FITC-labeled MSN with PICsome surface. Bare FITC-labeled MSN was assignable to peak (3’), considering its large negative zeta potential, and appeared at the same elution time with peak (3) in Figure II-5a. Sharp peaks found at ca. 4 min of elution time in Figure II-5a and b, i.e., peaks (2) and (2’), correspond to free-FITC. From the area-ratio of peaks (1) and (3), the efficacy of MSN loading was calculated to be ca. 83%. Such efficient loading of MSN without forming any aggregates can be explained by assuming the adsorption of cationic P(Asp-AP) on the surface of negatively charged MSN in the first step of MSN-encapsulated PICsome preparation shown in Figure II-2. First, cationic P(Asp-AP) is adsorbed on the negatively charged MSN surface. Then, PEG-PAsp is added, which preferentially formed PIC around the P(Asp-AP)-adsorbed MSN surface and facilitates the formation of MSN-encapsulated PICsomes. PEG-PAsp interacts with excess P(Asp-AP) remaining in the aqueous phase without adsorbing on MSN, forming a "unit PIC (u-PIC)", a unit of ion complex of P(Asp-AP) and PEG-PAsp by electrostatic interaction [II-15,II-17]. In brief, the formation of a PIC around the surface of P(Asp-AP)-adsorbed MSN by the addition of PEG-PAsp would an important factor in increasing the efficacy of MSN loading.

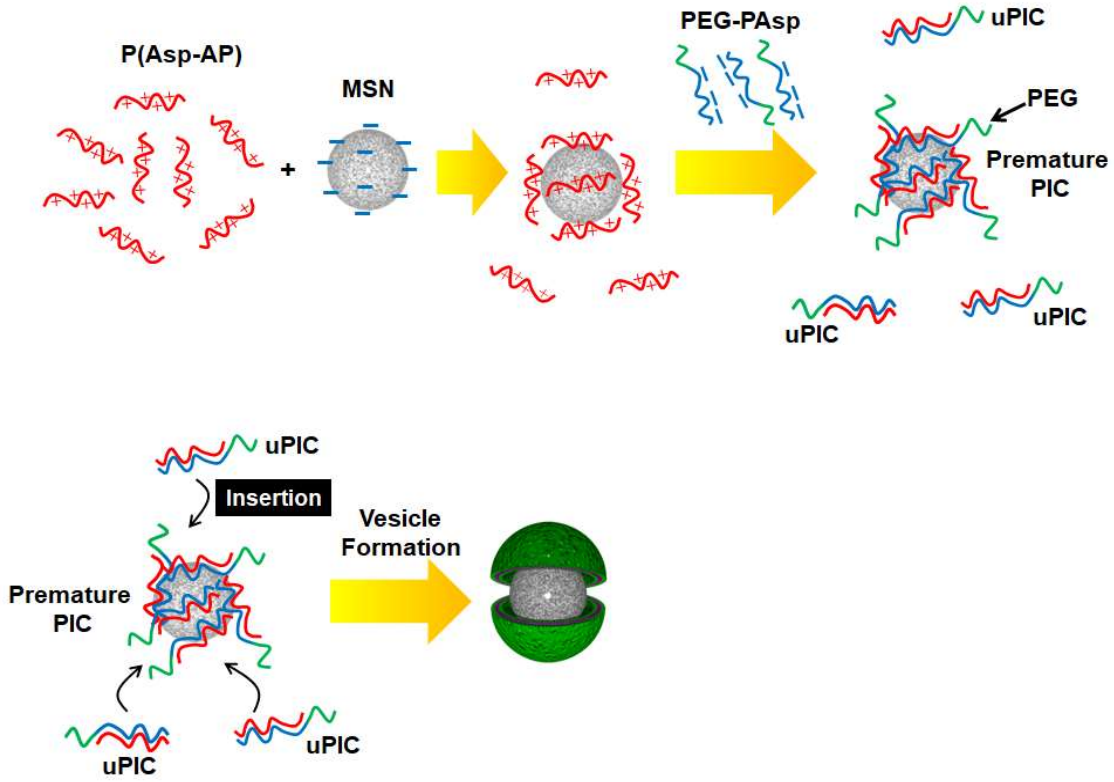

Figure II-2 Schematic illustration of preparation method of MSN-encapsulated PICsome.

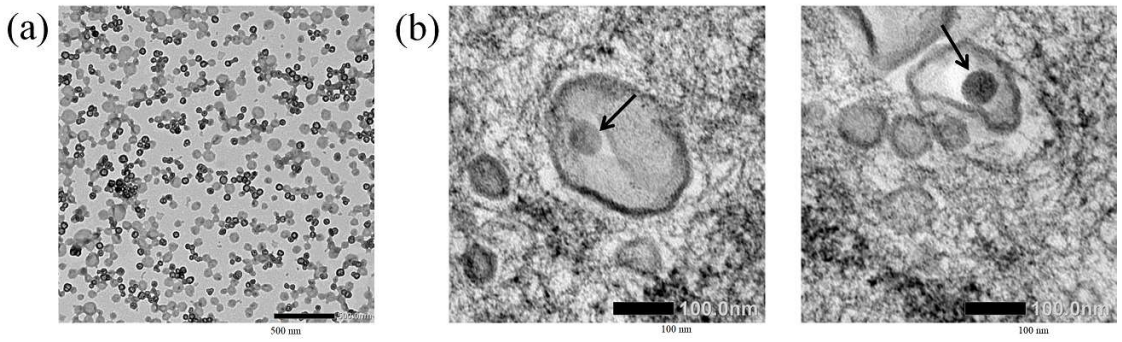

Figure II-3 (a) Conventional TEM image and (b) cross-sectional TEM images of MSN*@PICsome. Arrows indicate MSN.

Table II-1 The numbers of MSN@PICsome and empty PICsome counted using TEM images.

Image No.	MSN@PICsome (a)	Empty PICsome (b)
1	270	599
2	259	608
3	281	610
4	264	629
5	243	622
6	260	601
Total	1577	3669
particle number ratio of MSN@PICsome (a/a+b)		30%

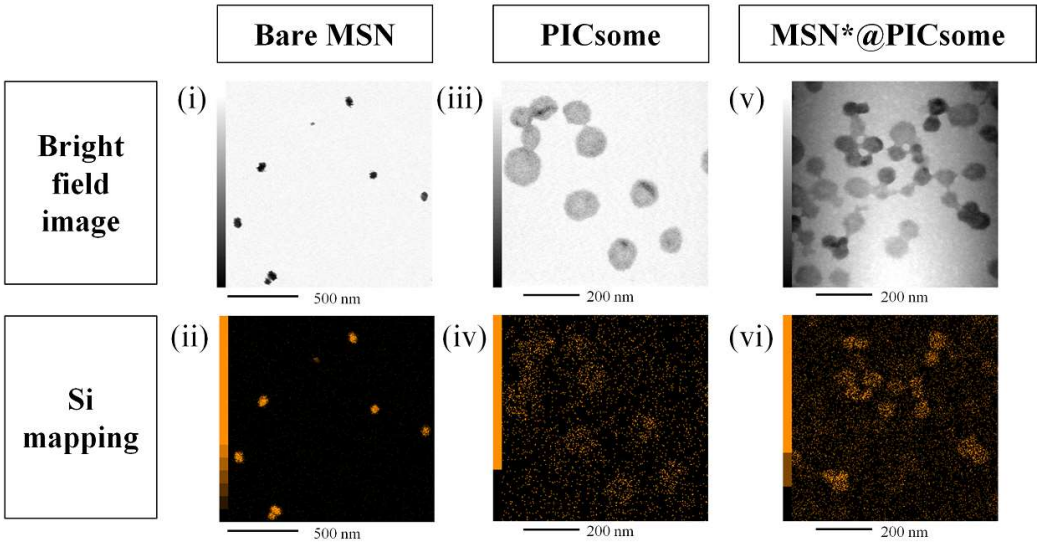

Figure II-4 Bright-field and Si-mapping images of (i, ii) bare MSN, (iii, iv) PICsome, and (v,vi) MSN*@PICsome. Si mapping was determined by energy dispersive X-ray spectroscopy (EDS) analysis (c-ii,iv,vi).

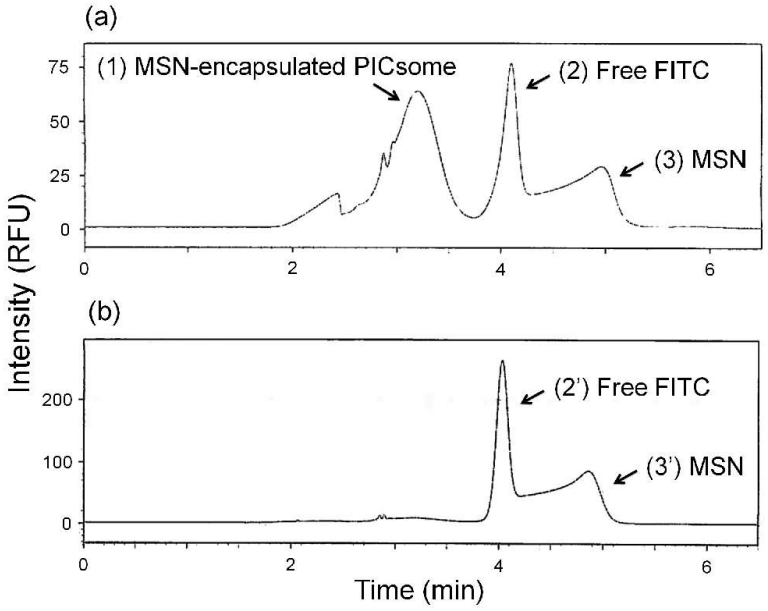

Figure II-5 Electropherograms of (a) as-prepared solution of MSN*@PICsome and (b) the mixture of MSN and PICsome solutions.

II.3.3. Surface Modification of MSN

The average zeta potentials of unmodified MSN, A-MSN, and S-MSN in 10 mM PBS (pH 7.4) were −18.1, 7.9, and −40.2 mV, respectively. These values are reasonable according to surface modifications. On the other hand, the average zeta potentials of MSN@PICsome, A-MSN@PICsome, and S-MSN@PICsome in 10 mM PBS (pH 7.4) were −2.8, −3.3, and −3.7 mV, respectively. There was no significant difference. These results suggest that charged MSN is encapsulated in the PICsome, neutral charged PEG layer on the PICsome surface affect the zeta potentials. However, it is need to testify directly that MSNs are modified after encapsulation in PICsome. Amino groups in A-MSN@PICsome were determined by TNBS assay, and sulfur atoms of sulfonic acid groups in S-MSN@PICsome were measured by EDS-FS. Only a few amino groups were detected in unmodified MSN@PICsome, while 8.9×10^{19} amino groups were detected in A-MSN@PICsome for 1 mg MSN. Furthermore, empty PICsomes treated with APTS using the same procedure as the modification of MSN@PICsome was measured by a TNBS assay, amino group was below the detection limit. This result indicates that the PICsome membrane is not modified by APTS. The intensity ratio of the S and Si peaks between S-MSN@PICsome and unmodified MSN@PICsome was very different (Figure II-6). The significantly higher S signal of S-MSN@PICsome clearly indicates successful modification of the functional group containing sulfur MSN@PICsome. Note that the empty PICsome treated with MPTS in the same manner as the modification of MSN@PICsome showed almost the same EDS spectrum as before the treatment, indicating that the PICsome membrane was not modified by the

MPTS treatment. Furthermore, the particle sizes were unchanged before and after modification (MSN@PICsome: 101 nm, PdI 0.08; A-MSN@PICsome: 105 nm, PdI 0.09; S-MSN@PICsome: 104 nm, PdI 0.08). From These results, surface modification of the encapsulated MSNs is possible without significantly changing of the MSN@PICsome.

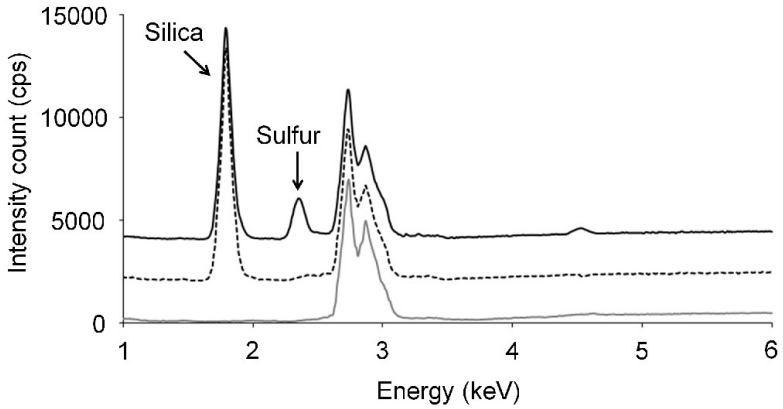

Figure II-6 EDS-FS spectra of MSN@PICsome (dotted line), S-MSN@PICsome (solid line), and empty PICsome after the treatment with MPTS (gray line).

II.3.4. Drug Absorption and Release Test

The LMWC retention capacity of A- and S-MSN@PICsome was compared by calculating the amount of adsorbed compound per MSN weight. RB was used as the anionic model compound with carboxyl groups; MSN@PICsome and S-MSN@PICsome adsorbed little RB (MSN@PICsome: 0.5w/w%, S-MSN@PICsome: 0.2 w/w%). On the other hand, A-MSN@PICsome showed a significant increase compared to the others, 3.2w/w%. This is likely due to the positively charged A-MSN, which increased adsorption through electrostatic interactions. Next, GEM, a widely used therapeutic agent for non-small cell lung cancer, was used as a cationic model compound; the adsorbed amount of GEM by MSN@PICsome and A-MSN@PICsome were both below the detection limit. On the other hand, S-MSN@PICsome was significantly improved, 7.9w/w%. Note that neither RB nor GEM could be retained in empty PICsomes, which is consistent with previous findings that PICsomes cannot retain LMWC [II-16,II-18].

Next, the release profile of GEM-S-MSN@PICsome was examined in 10 mM PBS (pH 7.4) and simulated body fluid (SBF, pH 7.4)(Figure II-7). The amount of GEM released in 72 h was only 10% in 10 mM PBS. In contrast, release was accelerated in SBF (pH 7.4), with just under 40% of GEM released after 72 hours. These results suggest that GEM-S-MSN@PICsome has practical properties, as its release may be inhibited under low ionic conditions during purification and storage, and enhanced under physiological conditions.

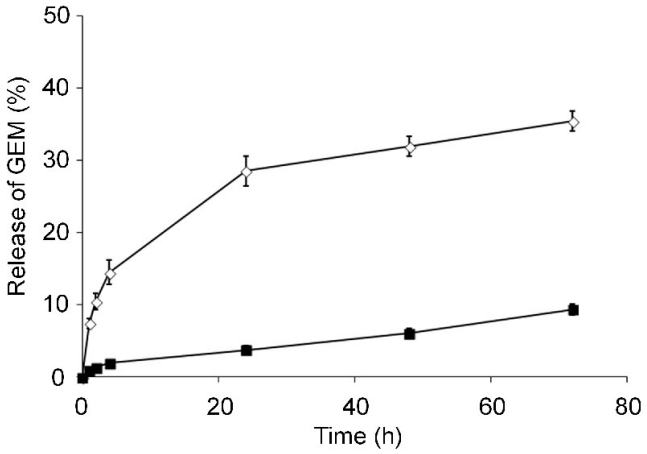

Figure II-7 Release profiles of GEM-S-MSN@PICsome in 10 mM PBS (pH7.4) (■) and in the SBF (pH7.4) (◇).

II.3.5. Cytotoxicity

The cytotoxicity of GEM-S-MSN@PICsome on A549 and C26 cells was evaluated using the samples listed in Table II-2. GEM-S-MSN@PICsome showed cytotoxicity to both A549 and C26 cells in time dependent manner, to a level as high as or slightly lower than that of GEM (group 6) alone and GEM-S-MSN (group 3)(Figure II-8). Formulations without GEM (Group 2, 4 and 5) showed negligible cytotoxicity to both cell lines, indicating that the cytotoxicity of GEM-S-MSN@PICsome is indeed due to GEM payload.

Table II-2 Composition of samples for the in vitro cytotoxicity and in vivo therapeutic experiments.

Group	Sample name	Contents		
		GEM	S-MSN	PICsome
1	GEM-S-MSN@PICsome	✓	✓	✓
2	S-MSN@PICsome	-	✓	✓
3	GEM-S-MSN	✓	✓	-
4	S-MSN	-	✓	-
5	PICsome	-	-	✓
6	GEM	✓	-	-

✓: include, -: not include

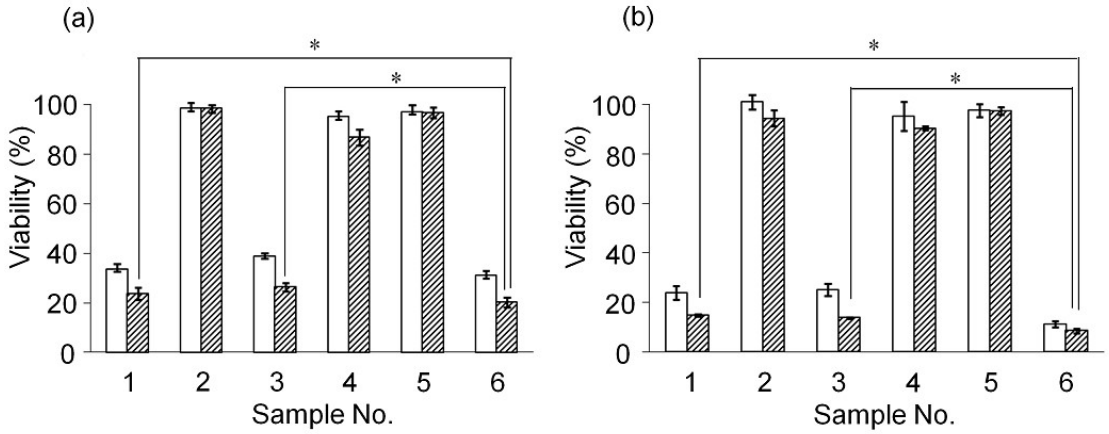

Figure II-8 Cytotoxicity against (a) A549 cells and (b) C26 cells over 48 h (open bar) and 72 h (slashed bar) periods. GEM concentration was adjusted at 0.01 μg/mL for C26 cells and 0.05 μg/mL for A549 cells, respectively. Sample 1, GEM-S-MSN@PICsome; sample 2, S-MSN@PICsome; sample 3, GEM-S-MSN; sample 4, S-MSN; sample 5, PICsome; and sample 6, GEM. *: $p < 0.05$.

II.3.6. Biodistribution

Plasma clearance of MSN@PICsome was evaluated before evaluating the pharmacokinetics. Cy5-labeled MSN (sample 1), Cy5-labeled MSN*@PICsome (sample 2), and Cy5-labeled empty PICsome (sample 3), Plasma clearance of these samples was compared. All PICsomes were cross-linked to increase their stability in the *in vivo* environment. The Cy5-labeled MSN*@PICsome contained both empty PICsomes (MSN@PICsome:Empty PICsome = 3:7 in particle number ratio based on TEM results) and MSN (MSN@PICsome:MSN = 83:17 in weight ratio based on CE. Results are shown in Figure II-9. The PICsome-based formulation showed significantly higher blood retention than free MSN. in Cy5-labeled MSN*@PICsome, Cy5 was adsorbed only on the silica surface of MSN and not labeled on the PICsome membrane. Thus, the data of sample 2 reflects the profile of free MSN and MSN@PICsome, excluding an influence from empty PICsome fraction. Apparently, the sample 2 revealed the longevity in blood retention comparable to the empty sample 3. Sample 1 (MSN) underwent the fast clearance from the blood (76% within 1 hour), indicating that the blood retention of Sample 2 is mainly due to MSN@PICsome. The slightly lower blood retention of Sample 2 compared to Sample 3 (87% versus 100%) can be explained by rapid elimination of free MSN from the blood.

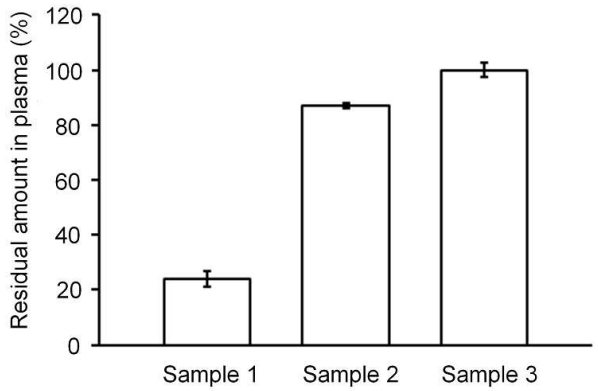

Figure II-9 Plasma clearance of Cy5-labeled free MSN (sample 1), Cy5-labeled MSN*@PICsome (mixture of Cy5-labeled MSN-encapsulated PICsome, Cy5-labeled free MSN, and empty PICsome without labeling) (sample 2), and Cy5-labeled empty PICsome (sample 3) measured at 1 h after administration into BALB/c mice.

To evaluate the utility of GEM-S-MSN@PICsome in the systemic treatment of solid tumors, its *in vivo* biodistribution in a mouse model of subcutaneous inoculated A549 lung tumors was examined. Biodistribution was evaluated by fluorescence determination of Cy5-labeled PICsome prepared with a polymer which attached Cy5 to the end of PEG-PAsp, or Cy5-labeled MSN prepared by Cy5 adsorbed on MSN. It is worth noting that release of Cy5 was suppressed under the SBF condition, and the amount of Cy5 released was less than 2% until 72 hours, which did not affect the biodistribution study (Figure II-10). All PICsomes were crosslinked. As a result, GEM-S-MSN@PICsome remained 10.8±0.4% in the blood at 24 hours after injection (Figure II-11a). In contrast, GEM-S-MSN remained negligible at 24 hours (0.9±0.1%). These results indicate that the encapsulation of GEM-S-MSN in the PICsome markedly improved its blood retention. The organ distribution and tumor accumulation are shown in Figure II-11b. tumor accumulation was remarkably improved for GEM-S-MSN@PICsome compared to GEM-S-MSN. This improved tumor accumulation can be explained by the EPR effect [II-19–II-21], which was observed for previously reported long circulating PICsomes so far reported [II-14,II-16,II-22–II-24].

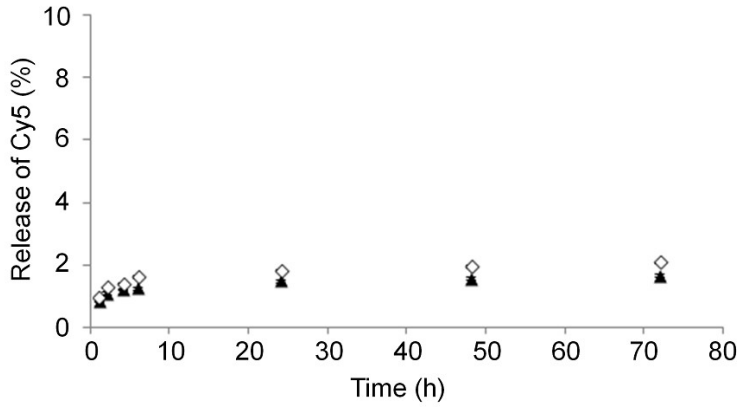

Figure II-10 Release profiles of adsorbed Cy5 dye from the Cy5-S-MSN@PICsome in 10 mM PBS (pH7.4) (▲) and in the SBF (pH7.4) (□) (n=3).

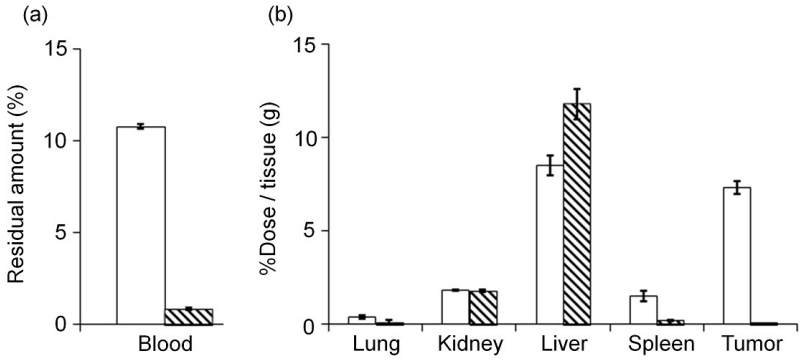

Figure II-11 Residual amount in (a) blood and (b) biodistribution of GEM-S-MSN@PICsome (open square) and GEM-S-MSN (slashed square) 24 h after i.v. injection.

II.3.7. In Vivo Therapeutic Efficacy

The therapeutic efficacy of GEM-S-MSN@PICsome was evaluated in a mouse model bearing subcutaneous A549 lung tumors. All formulations were administered every 7 days, and 3 times in total. All the drug-loaded formulation contained 5 mg/kg of GEM. At this dose of GEM, no significant weight loss was observed in all formulations. GEM, GEM-S-MSN, S-MSN, S-MSN@PICsome, and PICsome formulations showed no significant tumor growth suppression compared to the PBS group (Figure II-12). In contrast, mice treated with GEM-S-MSN@PICsome showed tumor growth suppression from 7 days after the first administration, and the difference in tumor volume between GEM-S-MSN@PICsome and the other formulations became significant with time. GEM-S-MSN@PICsome was improved tumor accumulation compared to the free GEM injection, and GEM release from GEM-S-MSN@PICsome occurred in sustained manner at physiological condition (Figure II-7). Resulting the increase of concentration of GEM in the tumor (or

increased AUC of GEM in the tumor) would lead *in vivo* good tumor suppression.

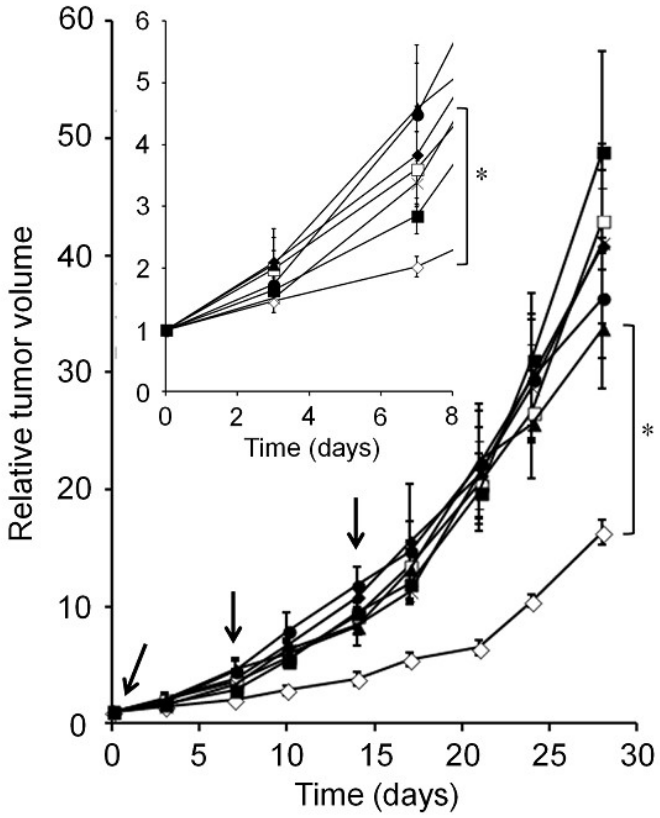

Figure II-12 Change in tumor volume with time for A549 bearing BALB/c nude mice after i.v. injection of GEM-S-MSN@PICsome (◊), S-MSN@PICsome (◆), GEM-S-MSN (□), S-MSN (■), PICsome (●),GEM (▲), and 10 mM PBS (pH7.4) (×). Each group included 5 mice. Administration started on day 0 and repeated on days 7 and 14 (indicated as an arrow in the figure). Tumor volume was measured twice a week until 28 days after injection. *: $p < 0.05$ (between ◇ and ▲).

II.4. Conclusion

Surface-charged nanoparticles, such as MSNs, can be encapsulated into PICsomes more efficiently by changing the order of polymer addition. MSN@PICsomes can be modified on the surface of encapsulated MSNs even after crosslinking to improve *in vivo* stability and can provide functionality according to the properties of the target compound. RB and GEM, which were used as model compounds, were adsorbed and retained by MSN@PICsomes with opposite charges and released in a sustained manner under physiological conditions. GEM-S-MSN@PICsomes showed similar blood circulation and tumor accumulation in mice as empty PICsomes, exhibiting good *in vivo*

therapeutic effects in C26-bearing mice.

I successfully prepared PICsome-based WLMWC sustained-release nanocarriers by utilizing inorganic adsorbents. I believe that this outcome provides new possibilities for PICsomes and enhances their value as DDS.

II.5. References

II-1. Yang, P.; Gai, S.; Lin, *J. Chem. Soc. Rev*. **2012**, 41, 3679−3698.

II-2. Fadeel, B.; Garcia-Bennett, A. E. *Adv. Drug Delivery Rev.* **2010**, 62, 362−364.

II-3. Mackowiak, S. A.; Schmidt, A.; Weiss, V.; Argyo, C.; Von Schirnding, C.; Bein, T.; Bräuchle, C. *Nano Lett*. **2013**, 13, 2576−2583.

II-4. Kecht, J.; Schlossbauer, A.; Bein, T. *Chem. Mater*. **2008**, 20, 7207−7214.

II-5. Zou, Z.; He, D.; He, X.; Wang, K.; Yang, X.; Qing, Z.; Zhou, Q. *Langmuir*. **2013**, 29, 12804−10.

II-6. Kim, J.; Kim, H. S.; Lee, N.; Kim, T.; Kim, H.; Yu, T.; Song, I. C.; Moon, W. K.; Hyeon, T. *Angew. Chem*., *Int. Ed*. **2008**, 47, 8438−8441.

II-7. Saikia, L.; Srinivas, D.; Ratnasamy, P. *Appl. Catal.*, *A*. **2006**, 309, 144−154.

II-8. Yamada, H.; Urata, C.; Aoyama, Y.; Osada, S.; Yamauchi, Y.; Kuroda, K. *Chem. Mater.* **2012**, 24, 1462−1471.

II-9. Zhang, H.; Dunphy, D. R.; Jiang, X.; Meng, H.; Sun, B.; Tarn, D.; Xue, M.; Wang, X.; Lin, S.; Ji, Z.; Li, R.; Garcia, F. L.; Yang, J.; Kirk, M. L.; Xia, T.; Zink, J. I.; Nel, A.; Brinker, C. J. *J. Am. Chem. Soc*. **2012**, 134, 15790−15804.

II-10. Alexander, R. L.; Greene, B. T.; Torti, S. V.; Kucera, G. L. *Cancer Chemother. Pharmacol*. **2005**, 56, 15−21.

II-11. Cullen, M. *Lung Cancer*, **2005**, 50, S5−S7.

II-12. Bunn, P. A., Jr.; Lilenbaum, R. *J. Natl. Cancer Inst*. ***2003***, 95, 341−343.

II-13. Cappuzzo, F.; Crino, L. *Expert Opin. Pharmacother*. **2002**, 3, 745−753.

II-14. Anraku, Y.; Kishimura, A.; Oba, M.; Yamasaki, Y.; Kataoka, K. *J. Am. Chem. Soc*. **2010**, 132, 1631−1636.

II-15. Chuanoi, S.; Anraku, Y.; Hori, M.; Kishimura, A.; Kataoka, K. *Biomacromolecules*, **2014**, 15, 2389−2397.

II-16. Anraku, Y.; Kishimura, A.; Kamiya, M.; Tanaka, S.; Nomoto, T.; Toh, K.; Matsumoto, Y.; Fukushima, S.; Sueyoshi, D.; Kano, M. R.; Urano, Y.; Nishiyama, N.; Kataoka, K. *Angew. Chem., Int. Ed*. **2016**, 55, 560−565.

II-17. Anraku, Y.; Kishimura, A.; Yamasaki, Y.; Kataoka, K. *J. Am. Chem. Soc*. **2013**, 135, 1423−1429.

II-18. Oana, H.; Morinaga, M.; Kishimura, A.; Kataoka, K.; Washizu, M. *Soft Matter*. **2013**, 9, 5448−5458.

II-19. Matsumura, Y.; Maeda, H. *Cancer Res*. **1986**, 46, 6387−6392.

II-20. Cabral, H.; Kataoka, K. *J. Controlled Release.* **2014**, 190, 465−76.

II-21. Cabral, H.; Miyata, K.; Kishimura, A. *Adv. Drug Delivery Rev*. **2014**, 74, 35−52.

II-22. Kishimura, A. *Polym. J*. **2013**, 45, 892−897.

II-23. Kokuryo, D.; Anraku, Y.; Kishimura, A.; Tanaka, S.; Kano, M. R.; Kershaw, J.; Nishiyama, N.; Saga, T.; Aoki, I.; Kataoka, K. *J. Controlled Release*. **2013**, 169, 220−227.

II-24. Anraku, Y.; Kishimura, A.; Kobayashi, A.; Oba, M.; Kataoka, K. *Chem. Commun*. **2011**, 47, 6054−6056.

Chapter III. CD@PICsomes for enzyme prodrug therapy prepared using a new encapsulation method, SWCL method

III.1. Introduction

The next objective of this study was to explore the possibility of utilizing the tumor-accumulating and semipermeable properties of PICsomes. This property renders PICsomes suitable for enzyme prodrug therapy (EPT). EPT involves the enzymatic conversion of inactive prodrugs into active drugs at target sites in the body. EPT has numerous advantages, including improved pharmacokinetics, enhanced absorption and stability, and reduced side effects. In particular, for drugs with potent pharmacological effects, such as anticancer drugs, it is necessary to deliver only a sufficient amount of the drug to the required part of the body, such as DDS or EPT, given that the systemic action of such drugs can cause severe side effects or make them unusable owing to toxic effects. Considering the use of PICsomes, prodrugs can be converted to an active drug only at the site where the enzyme-encapsulated PICsomes exist via the administration of small molecular weight prodrugs after delivering enzyme-encapsulated PICsomes to the target site. In other words, the drug effects do not occur at unnecessary sites, thereby reducing side effects. Furthermore, if the enzyme is active, drugs are continuously produced while the prodrug is being supplied. Recently, It was found that galactosidase-encapsulated PICsomes can be prepared by vortex mixing galactosidase and uncrosslinked PICsomes in water and that PICsomes accumulate in solid tumors after systemic administration in mice. Following the accumulation of galactosidase-encapsulated PICsomes in the tumor, the systemically administered fluorescent substrate molecules could be detected in the tumor for four days, enabling i*n vivo* fluorescence imaging [III-1]. This result suggests that enzyme-encapsulated PICsomes are promising nanocarriers for EPT.

However, low enzyme loading efficacy (the ratio of the loaded amount of enzyme to the total feed amount of enzyme) remains an issue for PICsome-based EPT applications; the loading efficacy is as low as 0.9% for galactosidase [III-2]. Improving the loading efficacy would be key for further development, not only because it enables efficient enzyme delivery but also because it leads to cost reduction. Therefore, it is necessary to increase the loading efficacy to prepare PICsomes with higher polymer concentrations. However, the polymer concentration affected the PICsome size. Therefore, the polymer concentration must be adjusted to prepare specific-sized PICsomes [III-3]. Another challenge is the small number of enzyme molecules that can be loaded into the internal cavity of PICsomes, with only one or two molecules of galactosidase loaded per PICsome [III-1,III-2]. Increasing the enzyme concentration during the loading process enhances the enzyme loading efficacy while increasing the viscosity and ionic strength of the solution, preventing the self-assembly of the PICsomes [III-3–III-7]. In the current study, a new loading method based on stepwise crosslinking of PIC membranes (the SWCL method) was developed to overcome the low loading efficacy of enzymes in PICsomes and the low enzyme activity per PICsome (i.e., a small number of loaded enzyme molecules). In the SWCL method, the first crosslinking step enhances the robustness of PICsomes during the loading process under high enzyme/charged polymer concentrations and high ionic strength

conditions. The second crosslinking step was performed to stabilize the PIC membrane *in vivo* and confine the loaded enzyme. After the second crosslinking step, the semi-permeability of the PICsome membrane was altered to render it suitable for EPT. Herein, I selected cytosine deaminase (CD) as the model enzyme for two reasons, the first of which was its physical properties. According to previous reports, CD (molecular weight, ~18 kDa) can permeate the PIC membrane after the first crosslinking but not after the second crosslinking, making it suitable for the SWCL method [III-6]. The second reason for selecting CD is functionality. CD converts 5-fluorocytosine (5-FC), a prodrug with low toxicity, into 5-fluorouracil (5-FU), a widely used anticancer drug. 5-FU is known to exert severe side effects owing to its nonspecific distribution in normal tissues following systemic administration [III-8–III-11]. In contrast, 5-FC has many advantages, such as a long blood half-life, low toxicity in humans, and low uptake into human cells [III-11], making it suitable as a prodrug. Therefore, I investigated CD-encapsulated PICsome (CD@PICsomes) for use in a CD/5-FC directed EPT system (Figure III-1).

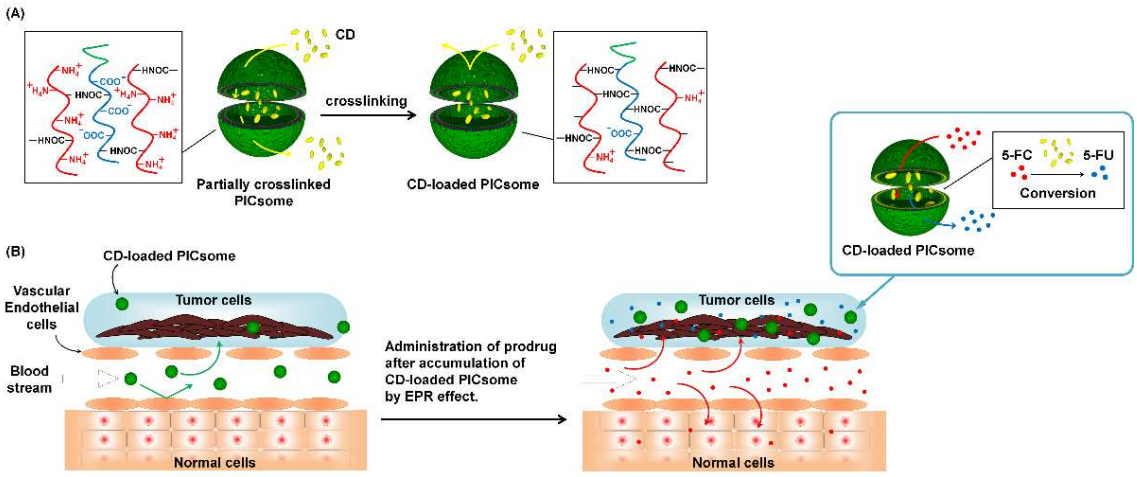

Figure III-1 Conceptual illustration of (A) a new strategy of enzyme loading into PICsome (SWCL method) and (B) its application to DEPT.

III.2. Material and Methods

III.2.1. Materials

Poly(5-aminopentyl-α,β-aspartamide) (P(Asp-AP)) with a degree of polymeriza-tion (DP) of 82 and poly(ethylene glycol) (PEG)-block-poly(α,β-aspartic acid) (PEG-PAsp, DP of PAsp = 75; Mn of PEG = 2,000, Mw/Mn of PEG = 1.05) were prepared as reported previously [III-12]. 1-Ethyl-3-(3-dimethylaminopropyl) carbodiimide hydro-chloride (EDC, Dojindo Molecular Technologies, Inc., Kumamoto, Japan), sulfo-Cy5 NHS ester (GE Healthcare Japan, Tokyo, Japan), Trypsin (Thermo Fisher Scientific Inc., Tokyo, Japan; used at 2.5%), 5-FC (Sigma-Aldrich Co. LLC., St. Louis, MO,

USA), 5-FU (Tokyo Chemical Industry Co., Ltd., Tokyo, Japan), and passive lysis buffer (Promega Co., Tokyo, Japan) were used as received. CD from yeast in 80% ammonium sulfate solution (CALZYME LABORATORIES, INC., San Luis Obispo, CA, USA) was used as received for all experiments, except to evaluate the interaction between the PIC membrane and CD. I prepared CD from yeast in 300 mM NaCl, 50 mM Tris-HCl, pH 8.0, and 10 mM dithiothreitol (DTT) to evaluate the interaction between the PIC membrane and CD.

III.2.2. Protein expression and purification

The open reading frame of the CD gene was codon-optimized for expression in *Escherichia coli* and subcloned into the *Nde*I and *Xho*I sites of pET-15b (GenScript, Piscataway, NJ, USA). His-tagged CD (His-CD) was expressed in *E. coli* BL21 (DE3)-RIL (Agilent, San Diego, CA, USA) with 0.5 mM isopropyl β-d-1-thiogalactopyranoside (IPTG) in LB Miller medium supplemented with 50 μg/mL ampicillin and 0.5 mM zinc-acetate at 16 °C for 16 h. Harvested bacteria were lysed in 50 mL lysis buffer (150 mM NaCl, 20 mM Tris-HCl, pH 8.0, 20 mM imidazole) by sonication using a UD-201 ultrasonic disrupter (Tomy Seiko Co. Ltd., Tokyo, Japan) at an output of 7 and 40% duty for three 5-min applications. The soluble lysate was fractionated by centrifugation at 16,000 rpm at 4 °C for 20 min and applied to a nickel-nitrilotriacetic acid (Ni-NTA) column containing 10 mL Ni-NTA superflow (QIAGEN, Valencia, CA, USA) equilibrated with lysis buffer. The column was washed with 100 mL wash buffer (150 mM NaCl, 20 mM Tris-HCl, pH 8.0, and 50 mM imidazole). Bound proteins were eluted with 100 mL elution buffer (250 mM NaCl, 20 mM Tris-HCl, pH 8.0, and 300 mM imidazole). His-tagged proteins were cleaved by thrombin using dialysis in dialysis buffer (250 mM NaCl, 20 mM Tris-HCl, pH 8.0) at room temperature for 3 h. Precipitation was observed during the dialysis. The precipitate was removed by centrifugation at 16,000 rpm for 30 min at 4 °C. The supernatant was applied to HiTrap Benzamidine FF (Cytiva, Marlborough, MA, USA) and Ni-NTA Superflow QIAGEN) columns, 1 and 2 mL, respectively. The flow-through was collected. After concentration to 20 mL by ultrafiltration with AmiconUltra (molecular weight cut-off [MWCO] 30,000; Merck, Kenilworth, NJ, USA), proteins were fractionated by size-exclusion chromatography (SEC) in SEC buffer (25 mM Tris-HCl, pH 8.0, 300 mM NaCl, 10 mM DTT) with Superdex 200 HiLoad 16-600 (Cytiva) at 1.5 mL/min using a BioLogic Duoflow FPLC system (Bio-Rad, Hercules, CA, USA). The final product was buffer-exchanged using ultrafiltration and concentrated to 10 mg/mL. The protein concentration was determined by the ultraviolet method using an extinction coefficient of 1.12 at 280 nm.

III.2.3. Material characterization

Dynamic light scattering (DLS) measurements were performed on a Zetasizer-nano (Malvern Instruments Ltd., Worcestershire, UK) to determine the particle size distribution. Transmission electron microscopy (TEM) was performed using a JEM-1400 microscope (JEOL Ltd., Tokyo, Japan) operating at 120 kV. The samples for TEM were dispersed in purified water and transferred onto 400 mesh size copper grids coated with a thin film of collodion and carbon, followed by staining with uranyl acetate. Fluorescence intensity was measured using a NanoDrop 3300 spectrophotometer (Thermo Fisher Scientific, Waltham, MA, USA).

III.2.4. Cell lines and animals

A549 human lung adenocarcinoma epithelial cells (National Cancer Center, Tokyo, Japan) and C26 murine colon adenocarcinoma cells (Alexandria Technical & Community College, Alexandria, MN, USA) were cultured in RPMI-1640 (Sigma-Aldrich) supplemented with 100 U/mL penicillin (Sigma-Aldrich), 100 μg/mL streptomycin (Sigma-Aldrich), and 10% fetal bovine serum (FBS) (Thermo Fisher Scientific). Female, 5-week-old BALB/c mice (Oriental Yeast, Tokyo, Japan) were used for *in vivo* experiments.

III.2.5. Preparation of CD@PICsomes

P(Asp-AP) and PEG-PAsp were separately dissolved in 10 mM phosphate buffer (PB, pH 7.4) at a final concentration of 1.0 mg/mL. Typically, PEG-PAsp solution (400 μL) was mixed with 530 μL of P(Asp-AP) solution to maintain an equal unit molar ratio of $–COO^-$ and $–NH_3^+$ in the mixed solution. The solution was mixed by vortexing at 2,000 rpm for 2 min to form PICsomes. For the first crosslinking, the reaction mixture was treated with 540 μL of 1.0 mg/mL EDC solution, which contained equal amount of EDC with the amount of $–COO^-$ in PAsp, left statically overnight at room temperature. The resulting solution was purified using a polyethersulfone (PES) ultrafiltration membrane (MWCO = 300,000) at 25 °C. The buffer exchange was repeated 10 times to completely remove byproducts from the reaction mixture, resulting in pre-crosslinked empty PICsomes (pCL-PICsomes). The final polymer concentration was adjusted to 10 mg/mL (10-fold dilution). The pCL-PICsomes were blended with 10 mg/mL CD solution (80% saturated ammonium sulfate solution) at a 5:8 volume ratio and then vortexed at 2,000 rpm for 2 min. The mixture was treated with 540 μL of 50 mg/mL EDC solution for the second-step crosslinking and incubated overnight at 4 °C. The resulting solution was purified using a PES ultrafiltration membrane (MWCO = 300,000) at 5 °C. The buffer exchange was repeated 10 times to completely remove byproducts and free CD from the solution, to yield CD-loaded PICsome (CD@PICsome).

To optimize the crosslinking conditions of pCL-PICsomes, four different EDC

concentrations were tested (1, 3 and 5 mg/mL). PCL-PICsomes were prepared using the same protocol with that of CD@PICsome, except for EDC concentrations. For reference CD loading experiments, the solutions of P(Asp-AP), PEG-PAsp, and CD (final CD concentration: 0.1–0.3 mg/mL) were mixed, or the P(Asp-AP) solution was mixed with the PEG-PAsp solution and then mixed with the CD solution (final CD concentration: 0.1–0.3 mg/mL).

III.2.6. Preparation of fluorescence modified CD-loaded PICsomes

To calculate the polymer concentration, Cy5-labeled pCL-PICsomes (Cy5-pCL-PICsomes) and CD@PICsomes with Cy5-labeling (CD@Cy5-PICsome) were prepared using Cy5-conjugated PEG-PAsp (PEG-PAsp-Cy5) instead of non-labeled PEG-PAsp, as previously reported[III-13]. To investigate the feed-to-loading efficiency (fLE) and leakage amount of CD, Cy5-labeled CD (Cy5-CD) were prepared from sulfo-Cy5 NHS ester and CD in 10 mM PB. The reaction mixture was purified by ultrafiltration using a PES membrane (MWCO = 3,000) to obtain Cy5-CD. The loading of Cy5-CD into PICsomes was performed using the same protocol with that of CD@PICsome, and four different concentrations of Cy5-CD were examined (1.0, 2.5, 5.0, and 10 mg/mL). To test the interaction between the PIC membrane and CD, Cy5-CD-loaded PICsomes (Cy5-CD@PICsomes) were prepared.

The PEG-PAsp-Cy5 concentration of PICsomes, Cy5-CD loading efficiency, and leakage amount of Cy5-CD from PICsomes were evaluated using a size exclusion chromatography (SEC) system equipped with a fluorescent detector (excitation/emission = 643/667 nm) and a Superdex 200 column (GE Healthcare, Chicago, IL, USA). As a mobile phase, 10 mM of phosphate buffered saline (PBS, pH 7.4) was used.

III.2.7. Interaction of pCL-PICsomes and CD

Enzyme activity was calculated from the conversion of 5-FC to 5-FU. The amounts of 5-FU and 5-FC were determined using a high-performance liquid chromatography system equipped with an ultraviolet detector (wavelength: 270 nm) and an ODS-3 C18 column (GL Sciences, Shanghai, China). A 19:1 mixture of 10 mM potassium dihydrogen phosphate and acetonitrile was used as the mobile phase. As a reference, CL Cy5-PICsomes were prepared as previously described [III-3]. To measure enzyme activity, CD@PICsomes were dispersed in 10 mM PBS (pH 7.4) to obtain a total polymer concentration of 14 mg/mL. A 20 μL of diluted CD@PICsome dispersion was mixed with 1.48 mL of 0.01 mg/mL 5-FC, and incubated at 40 °C. The conversion of 5-FC to 5-FU was determined at 10, 20, 30, 40, 50, and 60 min after mixing. To investigate the effect of CD concentration on the enzymatic activity of CD-loaded PICsomes, CD@PICsomes were prepared using four different CD concentrations (1.0, 2.5, 5.0, and 10 mg/mL). Then, each enzyme activity of obtained samples was

measured as shown above.

For further investigation, CD@PICsome were diluted to 0.2 mg/mL of polymer concentration. The diluted sample was mixed with 0.25% trypsin at a volume ratio of 1:1. The mixture was incubated at 37 °C for 5 min. then, enzyme activity of CD@PICsome treated with trypsin was measured by above method.

III.2.8. Evaluation of stability of CD@PICsome based on enzyme activity assay

To determine the polymer concentration, CD@Cy5-PICsome was used. To measure enzyme activity, the CD solution was diluted 100-fold with 10 mM PBS (150 mM NaCl, pH 7.4) to a final CD concentration of ~0.1 mg/mL. Enzyme activity of CD@PICsome was measured by the method described in 2.7. To confirm the stability of CD over the period used in the *in vivo* experiment (vide infra), the enzyme activities of CD@PICsome and CD were measured at 8, 16, 80, and 152 h after preparation (n = 3; initial enzyme activity adjusted to 0.47 U/mL at 40 °C for both cases). For the confirmation of durability against repeated use, the enzyme activity was measured for CD@PICsome at 40 °C (up to 10 runs for each CD@Cy5-PICsome; n = 3).

III.2.9. Evaluation of in vitro cytotoxicity

The cytotoxicity of the 5-FC and CD@PICsome combination was evaluated using A549 and C26 cells. Each cell line was seeded onto a 96-well plate (2.5×10^4 cells/mL) and pre-incubated with 90 μL of the culture medium for 24 h at 37 °C under a humidified atmosphere containing 5% CO_2. Subsequently, 5 μL of 0.2 U/mL CD@PICsome was added, followed by the addition of 5 μL of 0.04 or 0.08 mg/mL of 5-FC. As reference experiments, cells were treated with 5-FC (Table 1, samples 2 and 3), CD@PICsome (sample 1), or 5-FU (samples 6 and 7) at the same concentration as samples 4 or 5; 10 mM PBS (pH 7.4) was used as a negative control (sample 8). All samples were incubated in multi-well plates at 37 °C in a humidified atmosphere containing 5% CO_2. After a 48-h or 72-h incubation, viability was measured using a cell counting kit-8 (Dojindo Molecular Technologies, Inc., Rockville, MD, USA) by incubating for 1 h at 37 °C in a humidified atmosphere containing 5% CO_2. The absorbance of each well was measured at 450 nm using a model AD200 microplate instrument AD200 (Beckman Coulter Inc., Tokyo, Japan) (n = 3). Cell viability was calculated using the following formula:

$$\text{Cell viability (\%)} = \{[(A_{SAM}) - (A_{BLK})] / [(A_{PBS}) - (A_{BLK})]\} \times 100$$

where A_{SAM} is the absorbance of samples 1–7 in Table 1, A_{PBS} is the absorbance of the control PBS (sample 8), and A_{BLK} is the absorbance of the blank.

Table III-1. Treatment conditions for cytotoxicity evaluation

Sample	Contents		
	CD@PICsome	5-FC	5-FU
1	+	−	−
2	−	+ 2 μg/mL	−
3	−	+ 4 μg/mL	−
4	+	+ 2 μg/mL	−
5	+	+ 4 μg/mL	−
6	−	−	+ 2 μg/mL
7	−	−	+ 4 μg/mL
8	−	−	−

III.2.10. Evaluation of plasma clearance and biodistribution and hepatotoxicity of CD@PICsome

Each BALB/c mouse (n = 3) was subcutaneously inoculated with 100 μL of suspension of C26 cells in RPMI-1640 containing 10% FBS (1.0×10^6 cells/mL). The tumors were allowed to grow for 10 days. First, 200 μL of Cy5-CD@PICsome, which corresponded to 0.5 U/mL in 10 mM PBS (pH 7.4), was administered by intravenous (i.v.) injection through the tail vein of each mouse. At 24 and 72 h after injection, blood was collected from the postcaval vein using heparinized syringes, and the main organs (lung, kidney, liver, and spleen) and C26 tumor tissue were excised. After centrifugation of the collected blood at 20,000G for 5 min at 4 °C, the fluorescence of the plasma was measured using an Infinite M1000 pro microplate reader (Tecan, Männedorf, Switzerland). The main organs were homogenized with 5× passive lysis buffer (Promega KK., Tokyo, Japan). The resulting colloidal solutions were measured using a microplate reader (excitation and emission wavelengths of 643 and 667 nm, respectively).

To evaluate hepatotoxicity, C26-bearing mice were prepared (n = 3) and tumors were allowed to grow for 7 days. On day 1, 200 μL of 0.5 U/mL CD@PICsome in 10 mM PBS (pH 7.4) was administered by i.v. injection through the tail vein of each mouse. Then, 200 μL of 5-FC solution (10 mM PBS, pH 7.4; 5-FC concentration: 80 mg/kg) was similarly administered on days 4, 8, 11, and 15 (group 2 of Table 2). For comparison, mice were treated with CD@PICsome without further administration of 5-FC, 5-FU (80 mg/kg), 5-FC (80 mg/kg), or 10 mM PBS (pH 7.4) following the administration schedule shown in Table 2. Furthermore, 200 μL of blood was collected from the blood vessel under the chin using heparinized syringes 1 h after the injection of 5-FC, 5-FU, or 10 mM PBS. Plasma was collected by centrifugation at 20,000G for 5 min. Aspartate aminotransferase (AST), alanine aminotransferase (ALT), and alkaline phosphatase (ALP) levels were measured using a Dri-

Chem 7000z (FUJIFILM Corporation, Tokyo, Japan).

III.2.11. Evaluation of in vivo therapeutic effect

To evaluate *in vivo* therapeutic effect, C26-bearing mice were prepared as described above (n = 5). Tumors were allowed to grow for 7 days. Further, 200 μL of 0.5 U/mL CD@PICsome in 10 mM PBS (pH 7.4) was administered by i.v. injection through the tail vein of each mouse on day 1. Subsequently, 200 μL of 5-FC solution (10 mM PBS, pH 7.4) was administered by i.v. injection on days 4, 8, 11, and 15 (Table 2, groups 1 and 2). As a positive control, 5-FU was similarly injected without the administration of CD@PICsome (Table 2, groups 3 and 4). As negative controls, mice were treated with CD@PICsome (Table 2, group 5), 5-FC (groups 6 and 7), and 10 mM PBS (pH 7.4; group 8). Two different concentrations (10 and 80 mg/kg) were administered. Mouse body weight and tumor size were measured twice a week (on days 1, 4, 8, 11, 15, 18, 22, 25, and 29). The tumor size was determined using a digital Vernier caliper across its two perpendicular diameters. Tumor volume (V) in mm^3 was calculated as:

$$V = (a^2 \times b)/2$$

where *a* and *b* are the minor and major diameter of the tumor, respectively.

Mouse body weight and tumor size were monitored until the tumor size was > 2500 mm^3 and weight loss was > 25%. Mice that met either of the criteria were sacrificed. the experiment was completed when three mice died or were euthanized in the group.

Table III-2. Administration schedule for in vivo therapeutic experiment.

Group	Day				
	1	4	8	11	15
1	×	♦	♦	♦	♦
2	×	◊	◊	◊	◊
3	–	■	■	■	■
4	–	□	□	□	□
5	×	–	–	–	–
6	–	♦	♦	♦	♦
7	–	◊	◊	◊	◊
8	Δ	Δ	Δ	Δ	Δ

×: CD@PICsome, ♦: 10 mg/kg of 5-FC, ◊: 80 mg/kg of 5-FC, ■:10 mg/kg of 5-FU, □: 80 mg/kg of 5-FU, Δ: 10 mM PBS (pH 7.4)

III.2.12. Statistical analysis

The calculation of mean value and standard deviation in figures, regression analysis, and Student's t-test were conducted using an Excel software, version 2011 (Microsoft, Washington, United States). For the t-test performed in cytotoxicity and therapeutic assays, a p value < 0.05 was considered statistically significant.

III.3. Results and discussion

III.3.1. Preparation of crosslinked PICsomes loaded with CD (CD@PICsomes) by SWCL method

Increasing the loading amount and feed-to-loading efficiency (fLE) of enzymes into PICsomes is key to their practical use in DEPT. The minimum fLE of enzymes in PICsomes using the conventional method of vortex mixing was limited to <1%. In the conventional method, enzyme molecules and pre-assembled empty PICsomes are mixed, followed by vortex mixing to disassemble the PICsomes into u-PICs [III-14]. The PIC structure comprises polyanions and polycations with minimal association to compensate for their charge. After the vortex mixing is stopped, PICsomes spontaneously regenerate through the self-assembly of unit PICs. This regeneration allows the entrapment of enzymes that are in the solution [III-1]. The process of enzyme entrapment proceeds stochastically, which results in not enough loading efficacy to apply to DEPT. The loading efficacy can be improved by increasing the concentration of the polymer and enzyme in the solution. In the present study, the conventional method did not work properly for CD loading at higher enzyme concentrations in the polymer system (P(Asp-AP)/PEG-PAsp), resulting in the formation of micrometer-sized aggregates. Presumably, the high salt concentration of the CD stock solution (80% saturated ammonium sulfate solution; final concentration of ammonium salt is approximately 0.5 g/mL) may hamper the stable polyion pairing in the mixed enzyme–polymer solution. In fact, under higher salt concentration conditions, robust polyion pairing is required to keep the unilamellar structure and well-controlled size of the PICsome [III-4,III-7].

In the SWCL method, the first step involves loose crosslinking to maintain the unilamellar PICsomes with a well-controlled size against environmental stresses (viscosity and ionic strength) [III-14]. The second step involves crosslinking that stably confines the loaded enzymes into the inner cavity while maintaining the proper semipermeable nature of the PICsome membranes, and stably exist in *in vivo* environment. As previously reported, PIC membranes with a lower degree of crosslinking can have higher permeability, which allows the permeation of macromolecules, such as linear PEG with a molecular weight (M.W.) of 42,000 and branched PEGs with an M.W. of 10,000. In the case of branched PEGs with a hydrodynamic radius of 2.5–2.7 nm, which were loaded into PICsomes with lower crosslinking, approximately 15% of release occurred over 1 week [III-6].

Therefore, CD with an approximate M.W. of 18,000 (2.0 nm calculated hydrodynamic radius [III-15]) would permeate the PICsome membrane. In addition, to enhance the quantity of CD loaded into pCL-PICsomes, loading could be performed in the presence of a high concentration of PICsomes, enzymes, and salt. pCL-PICsomes are considered to be stable in these harsh conditions. Moreover, the second crosslinking suppressed the leakage of CD from the PICsomes. Thus, the SWCL method appears effective for loading and maintaining enzymes inside PICsomes.

First, Pre-CL PICsomes were prepared with an amount of EDC equal to the carboxyl groups in the polymer. This crosslinking treatment was identical to the method I previously reported, in which PICsomes with a crosslinking degree of 45% that were obtained displayed a permeation of linear PEG with an M.W. of 42,000, and branched PEGs with an M.W. of 10,000 [III-6]. The second crosslinking treatment was performed using a 50-fold EDC to the original amount of carboxyl groups in the polymer, in which the crosslinking degree of PICsomes was estimated to be ~90% [III-6]. Such a higher crosslinking degree would contribute to the prevention of leakage of loaded CDs. The fLE of CD@PICsomes was confirmed by GPC using Cy5-CD@PICsomes without purification. The fLE (%) was calculated as follows:

$$\mathrm{fLE}(\%) = \frac{Peak\ area\ of\ (1)}{Sum\ of\ peak\ area\ (1) and\ (2)} \times 100$$

The fLE of CD@PICsome was approximately 9% 1 h after the addition of the CD solution (GPC data not shown) and 19% after 24 h (GPC data not shown). This fLE was considerably higher than that reported for previous enzyme-loaded PICsomes (fLE < 1%) [III-1,III-2,III-16]. However, this loading method is time-consuming and may cause the deactivation of the enzyme. Therefore, I decided to use vortex mixing to facilitate enzyme loading. Surprisingly, two minutes of vortex mixing for CD loading enhanced the fLE to 44% (Figure III-2A and Figure III-3). Peak (1), which was eluted at the same elution time as Cy5-labeled empty PICsomes, is assignable to Cy5-CD@PICsome. Peak (2) was assigned to a free Cy5-CD. Notably, the CD content of the CD@PICsome formulation was estimated to be ~41 w/w% based on the fLE value. Thus, enzyme activity-based loading efficiency (LE) was calculated from the enzyme activity measurements. I estimated the enzyme activity using “Unit (U)” as an indicator (1 U is defined as the amount of enzyme that converts 1 μmol of substrate per minute at 40 °C). The enzyme activity of the obtained CD@PICsome was 16 U, while the enzyme activity of the CD used for loading was 60 U, indicating that 27% enzyme activity was maintained. Considering the fLE of 44%, ~40% of enzyme activity was lost, probably due to deactivation by the chemical influence of EDC and/or physical impact imposed during the encapsulation and purification processes. It is noteworthy that DLS measurements revealed no significant difference in the average size and polydispersity index (PDI) before (size = 101 nm, PDI = 0.06) and after (size = 105 nm, PDI = 0.08)

CD loading treatment via vortex mixing. In addition, no significant difference was observed in the morphology of the particles before and after the CD loading treatment (Figure III-2B). Thus, the vortex-based SWCL method was helpful for the enhancement of fLE and enzyme content without deterioration, and in further experiments, I decided to use the vortex-based method.

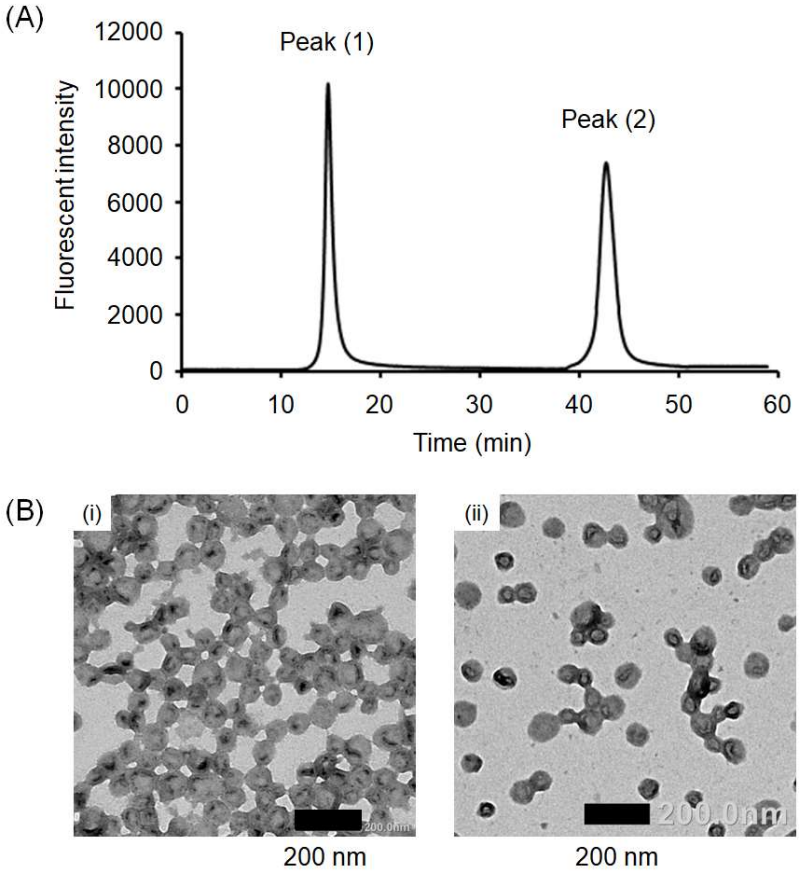

Figure III-2. Characterization of CD@PICsome. (A) SEC chromatogram of Cy5-CD@PICsome without purifi-cation. (B) TEM images of pCL-PICsome (i) and CD@PICsome prepared by the SWCL method (ii).

Collectively, the SWCL method provides more options for enzyme loading conditions by improving PICsome stability via the first crosslinking step and suppressing payload leaching by the second crosslinking step. However, the SWCL method is limited in that it does not allow the loading of enzymes exceeding a certain M.W. Concerning enzymes previously used as PICsome cargoes [III-1,III-2,III-16], the SWCL method is suitable for lysozyme (~14,000) and asparaginase (~40,000), but not β-gal (~540,000). This is because if the molecular weight of payloads is too large, payloads cannot penetrate the membrane of the pCL-PICsome.

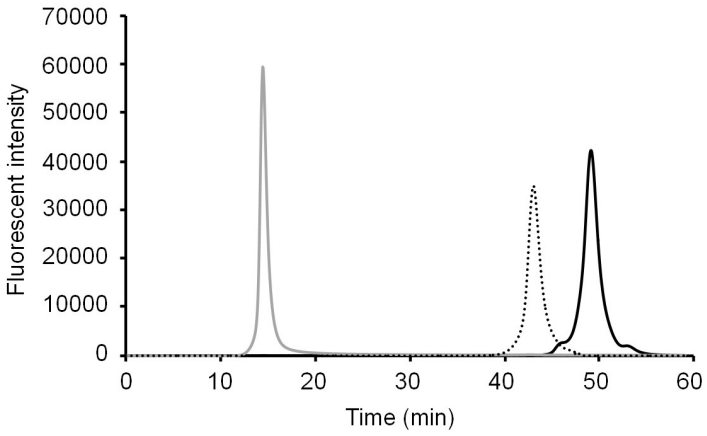

Figure III-3. SEC chromatograms of Cy5-CD (dotted line), crosslinked Cy5-PICsome (gray line) and Cy5 (solid line).

III.3.2. Interaction of pCL-PICsomes and CD

The fLE value found for the SWCL method was >50 times higher with vortex mixing than the estimated value of 0.8%.

Assuming that the density of the PIC membrane is 1.

According to the diameter of the PICsome is 105 nm and the thickness of the PIC membrane is 10 nm,

The calculated volume of one PICsome is 192938π nm^3,

The calculated inner volume of one PICsome is102354π nm^3,

Thus, the membrane volume of one PICsome is estimated of 90584π nm^3.

3.8 mg/mL (total polymer concentration at the CD encapsulation process) of PICsome particles with 90584π nm^3 is existed in 1 cm^3 (=10^{21} nm^3) of solvent, the weight ratio of PIC membrane is 0.0038.

Since the density is 1 g/mL, the estimated number of particles is

$10^{21}/90584\pi \times 0.0038 = 4.195 \times 10^{13}/\pi$

The estimated volume of $4.195 \times 10^{13}/\pi$ PICsomes is

$4.195\times10^{13}/\pi \times 192938\pi = 8.094 \times 10^{18}$ nm^3

This volume is converted to the volume ratio, which value is

$8.094 \times 10^{18}/10^{21} \times 100 = 0.80\%$

From this calculated value, the contribution from the mechanical impact of the vortex mixing is limited (~2.3-fold increase for the SWCL without vortex mixing), and it is reasonable to assume that the condensation of CD occurred in the PICsome compartment regardless of the mechanical impact from the vortex mixing. One possible explanation is the interaction between CD and the PIC membrane. Thus, treatment of CD@PICsome with trypsin was performed to determine the location of CD. Trypsin

treatment resulted in a loss of approximately 70% of the enzyme activity. The M.W. of trypsin (23,000) rendered it incapable of permeating the PIC membrane after the second crosslinking. Therefore, ~70% of the loaded CD would interact with the PIC membrane, which contributed to the inactivation of CD by trypsin.

To gain more insight into the interaction of CD with Pre-CL PICsomes, the effect of CD concentration on fLE during the CD loading process was investigated using Cy5-CD. The CD concentration and fLE showed a good linear relationship (Figure III-4 and Figure III-5). This result suggests that a higher concentration of CD accelerates the encapsulation process (Figure III-4B). One possible explanation for the accumulation of CD in the membrane is the electrostatic interaction and/or hydrophobic interaction. In addition, the PIC membrane may show an upper limit for the accommodation of CD because of its limited space, with a plateau in the amount of CD in the membrane. However, such an upper limit was not found in this CD concentration range. This finding indicates that only a rising part of the curve was observed in the range of this experiment (Figure III-4B). The fLE value obtained in this section (29% for 10 mg/mL CD solution) was lower than the values in the previous section (44%). Plausible factors include different sources of CD (in this section, I prepared CD, while for the experiment in the previous section, I used a commercially available CD), and the difference in solution composition (the product in the present study was dispersed in 25 mM Tris-HCl, pH 8.0, 300 mM NaCl, 10 mM DTT; the commercial product was dispersed in 80% saturated ammonium sulfate solution).

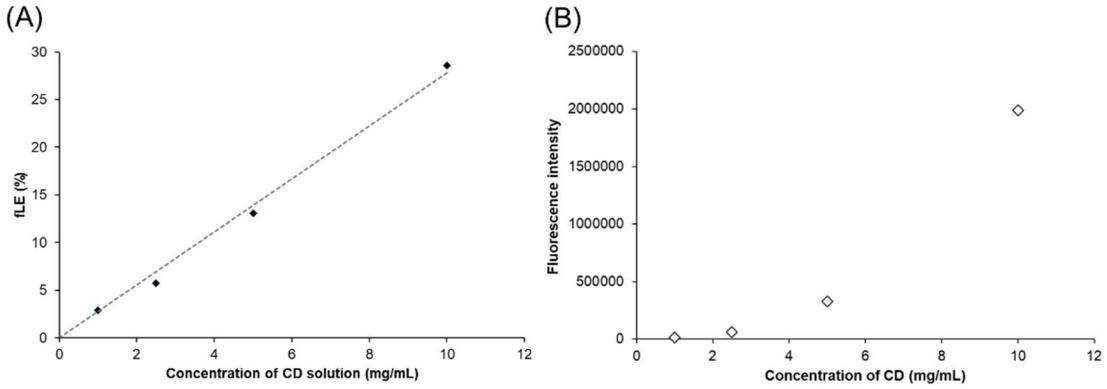

Figure III-4. CD concentration dependency of fLE (A) and CD loading amount (B).

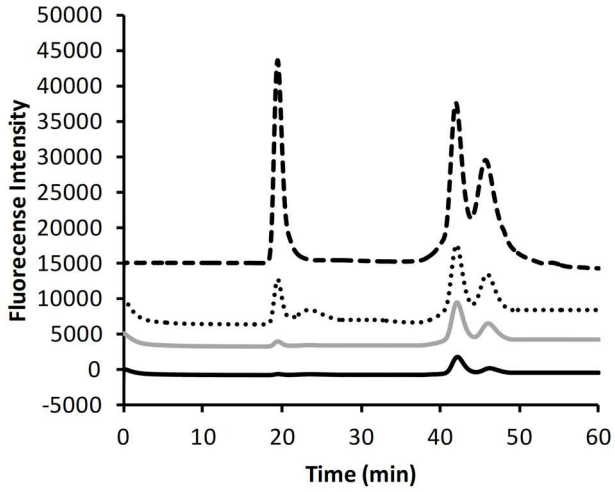

Figure III-5. SEC chromatograms of the reaction mixture after the vortex-driven loading and 2nd crosslinking treatment obtained at various concentrations of Cy5-CD: 10 mg/mL (black dotted line), 5.0 mg/mL (gray dotted line), 2.5 mg/mL (gray solid line), and 1.0 mg/mL (black solid line).

The average particle size of the Pre-CL PICsomes used in this section was 135 nm, and the average particle size of CD@PICsome was 147 nm. Assuming a PIC membrane thickness of 15 nm [III-12], the volume expansion rate of the PIC membrane was 121%. According to the fLE value of 29% for 10 mg/mL CD (Figure 2), 4.6 mg of CD was loaded per 10 mg of polymer, and 3.2 mg of CD was assumed to be in the membrane, based on the 70% activity loss by trypsin treatment. The remaining 30% of CD would be out of the trypsin permeable area.

Next, the effect of the feed concentration of CD on the enzyme activity of CD@PICsomes was investigated using CD without Cy5 labeling (Figure III-6). Negligible enzyme activity was observed for the products obtained at a feed CD concentration of 2.5 mg/mL, whereas much higher activity was confirmed in the case of a feed CD concentration >2.5 mg/mL. A possible explanation for this difference is the inactivation of CD by the EDC treatment used for the second crosslinking. In fact, the EDC used for the second crosslinking was in excess of the total number of carboxylate groups in the PICsome membrane. Therefore, it is conceivable that the residual EDC reacted with CD, resulting in its deactivation. This effect would be more remarkable at lower CD concentrations.

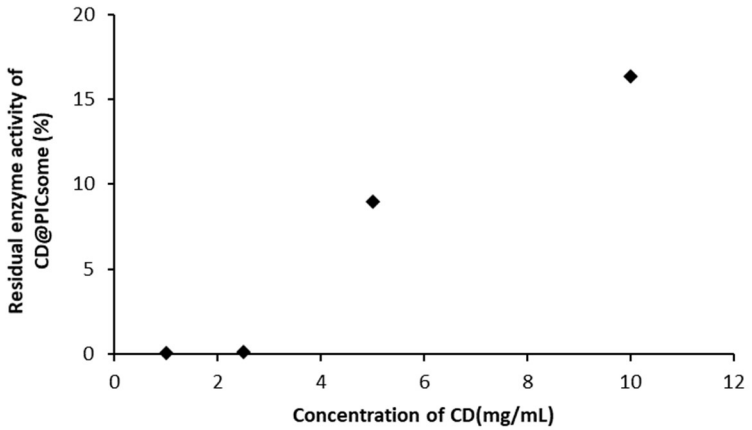

Figure III-6. CD concentration dependency of residual enzyme activity of CD@PICsomes after the second crosslinking.

III.3.3. Stability of CD@PICsome based on enzyme activity

The enzyme activity change of CD@PICsome was tested in 10 mM PBS at 40 °C, which is the typical body temperature of a mouse (Figure III-7). The free CD was completely deactivated within 72 h, whereas CD@PICsome maintained 50% of the initial enzyme activity even after 150 h. The enzyme activity change of CD@PICsome and 5-FU production for repetitive use were measured (Figure III-7B and C). The enzyme activity of free CD decreased in proportion to the increase in run number and was completely deactivated after ≥ 6 runs. On the other hand, the enzyme activity of CD@PICsome was almost constant over 10 runs, and CD@PICsome lasted till the production of 5-FU. These results indicate that CD was stabilized by loading into PICsomes, which can contribute in prolonging enzyme activity lifetime and increasing durability. A confined environment provided by PICsomes may contribute to the protection of enzymes from deactivation [III-1,III-2,III-4,III-16]. Thus, CD@PICsome is expected to be more stable and would work continuously under in vivo conditions. Notably, CD stabilized by the protection of PICsomes leads to the possibility of storage under milder conditions and does not need to be stored at low temperatures.

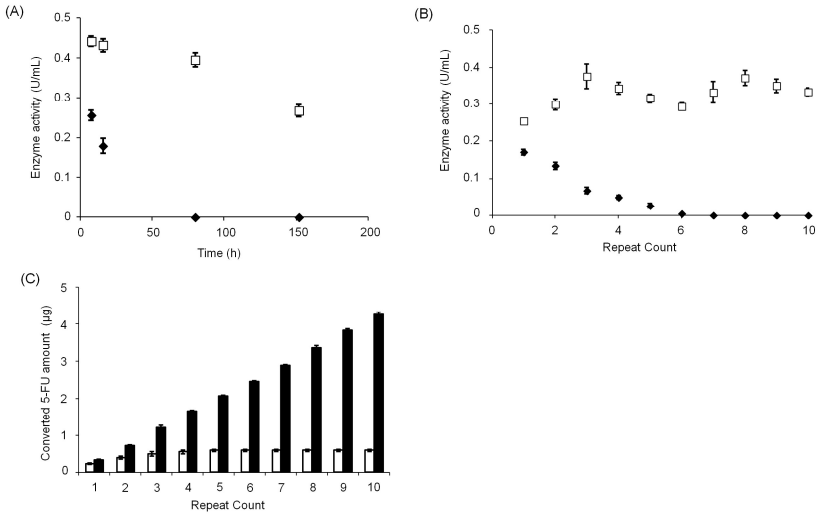

Figure III-7. Stability of CD@PICsome. (A) Time-dependent enzyme activity change of free CD and CD@PICsome in 10 mM PBS (pH 7.4) at 40 °C (open square: CD@PICsome, closed square: free CD). The X-axis represents the starting time of enzyme activity measurement from the en-zyme-containing sample preparation. (B) Enzyme activity change of free CD and CD@PICsome for repetitive use at 40 °C (open square: CD@Cy5-PICsome, filled square: Free CD). (C) Amount of 5-FU produced with the repetitive use of CD (filled bar: CD@Cy5-PICsome, open bar: Free CD).

III.3.4. Evaluation of cytotoxicity of CD@PICsome

Before proceeding to the *in vivo* experiments, the *in vitro* cytotoxicity of CD@PICsome was examined (Figure III-8). Cell viability was not affected by 5-FC or CD@PICsome (sample No. 1–3). On the other hand, significant cytotoxicity was observed after co-treatment with CD@PICsome and 5-FC (sample No. 4 and 5), comparable to that of 5-FU treatment (sample No. 6 and 7). Slightly lower cytotoxicity was observed for the CD@PICsome and 5-FC co-treatment after 72 h. This can be attributed to the gradual deactivation of CD, as shown in Figure III-7A. Thus, cytotoxicity was successfully confirmed when 5-FC and CD@PICsome co-existed, and the enzyme nanocarriers and prodrugs were not harmful in terms of acute toxicity. Considering that 5-FC is not transported into the cytoplasm through the plasma membrane, its conversion to 5-FU by CD@PICsome likely occurred in the extracellular medium [III-17].

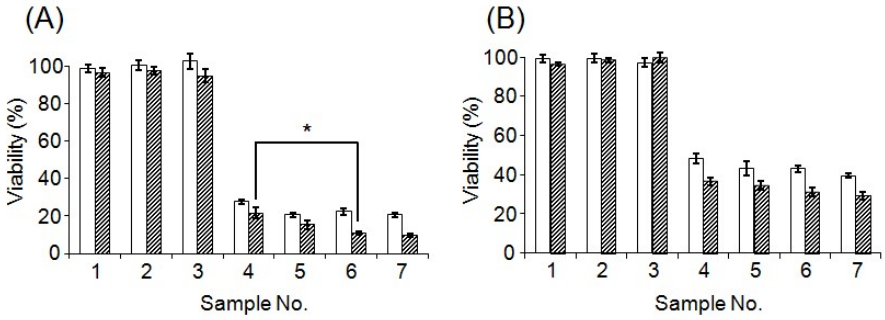

Figure III-8. Cell viability after treatment with 5-FC, 5-FU, and CD@PICsome: (A) C26 cells, and (B) A549 cells (open bar: 48 h after addition of samples, slashed bar: 72 h after addition of samples). Sample 1: CD@PICsome (0.01 U/mL), sample 2: 5-FC (2 μg/mL), sample 3: 5-FC (4 μg/mL), sample 4: CD@PICsome (0.01 U/mL) and 5-FC (2 μg/mL), sample 5: CD@PICsome (0.01 U/mL) and 5-FC (4 μg/mL), sample 6: 5-FU (2 μg/mL), sample 7: 5-FU (4 μg/mL). *$p < 0.05$ (between sample 4 and 6 at 72 h). The values in parentheses represent concentrations of CD, 5-FC, or 5-FU in each well.

III.3.5. Evaluation of plasma clearance, biodistribution, and hepatotoxicity of CD@PICsome

The biodistribution of Cy5-CD@PICsome was investigated to gain more insight into the therapeutic application of CD@PICsome. Regarding the plasma clearance of Cy5-CD@PICsome, residual fraction to the dose were 14.9% and 9.4% in blood at 24 and 72 h after injection, respectively. The order of organ uptake of Cy5-CD@PICsome was, liver > C26 tumor ~ spleen >> lung and kidney (Figure III-9). These findings indicated that accumulation of Cy5-CD@PICsome preferentially occurred in tumor tissues of major organs other than the liver. Similar prolonged blood circulation time and tumor accumulation behavior were observed for previously reported PICsomes, indicating that CD@PICsome did not lose its pharmacokinetic advantage compared to previous PICsomes, even after loading a large amount of enzyme [III-12,III-16,III-18].

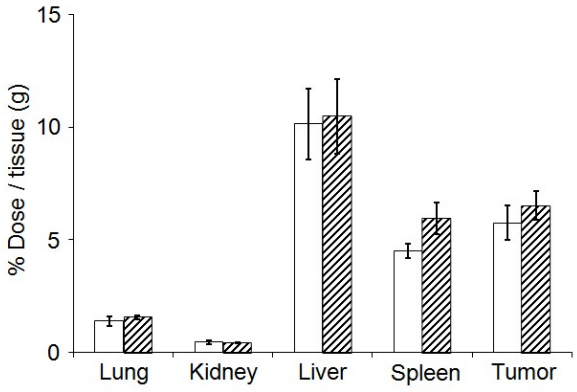

Figure III-9. Biodistribution and tumor accumulation of Cy5-CD@PICsome (open square: 24 h after injection, slashed square: 72 h after injection).

Based on the biodistribution results, CD@PICsome accumulation occurred most frequently in the liver. Therefore, hepatotoxicity after administration of CD@PICsome and 5-FC was investigated. The values of AST, ALT, and ALP for group 2 (CD@PICsome and 80 mg/kg 5-FC) were similar to those of the other control groups (Figure III-10). These results clearly show that the EPT of CD@PICsome and 5-FC does not damage the liver and can be safely used for therapeutic purposes. The impermeability of 5-FC to the cell membrane may suppress its conversion from 5-FC to 5-FU in the liver.

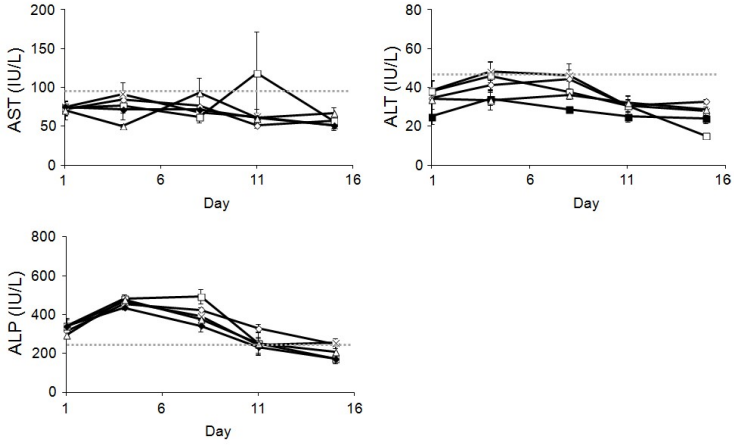

Figure III-10. Hepatotoxicity of EPT based on CD@PICsome and 80 mg/kg of 5-FC (◊, group 2), 10 mg/kg of 5-FU (■, group 3), 5-FU (□, group 4), CD@PICsome (×, group 5), 5-FC (○, group 7) and 10 mM PBS (pH 6.8) (Δ, group 8). The gray dotted line represents the average value for normal female BALB/c mice.

III.3.6. Evaluation of in vivo therapeutic effect of CD@PICsome

Next, CD@PICsome was used for *in vivo* experiments using tumor-bearing mice. In fact, PICsomes with a diameter of 100 nm showed selective accumulation in C26 tumor tissues due to the EPR effect [III-12]. I planned the experiment as follows (Table III-2). First, C26 tumor cells were subcutaneously inoculated as a model tumor. Then, CD@PICsome was administered on day 1. A 3-day period followed so that CD@PICsome could accumulate in the tumor tissue by the EPR effect and gets eliminated from the bloodstream [III-1]. Finally, 5-FC was administered on days 4, 7, 11, and 14 at different concentrations (group 1, 10 mg/kg; group 2, 80 mg/kg). As a control, only PBS was administered (group 8; negative control).

Remarkably, after CD@PICsome administration, significant tumor growth suppression was confirmed for the dose condition of 10 mg/kg of 5-FC from day 8 (Figure III-11A, group 1), although the therapeutic effect was hardly observed for the 5-FC and CD@PICsome administration groups (Figure III-11B, groups 5 and 6). These results suggested that the DEPT system worked well *in vivo*. Moreover, group 1 showed a superior therapeutic effect compared to the group 3. In addition, an obvious delay in the onset of weight loss and significant suppression of weight loss were confirmed for group 1, whereas group 3 showed limited suppression of weight loss (Figure III-14). This result can be mainly explained by the prolonged blood half-life of 5-FC (3–4 h [III-11]) compared to that of 5-FU (8–20 min [III-10]), which allows for the lasting conversion of 5-FC to 5-FU by CD@PICsome at the tumor site.

In the case of the 80 mg/kg dose, group 4 (treated with 5-FU) showed a remarkable antitumor effect. However, all mice died before day 15 (Figure III-12A). This side effect was more serious than that in group 3 (low-dose condition). Notably, group 2 (treated with CD@PICsome and 5-FC) showed apparent tumor growth suppression compared to the PBS group (Figure III-13), and negligible body weight loss on any day despite tumor growth (Figure III-14). This indicates a better prognosis after co-treatment with CD@PICsome and 5-FC. In particular, the antitumor effect of group 2 was comparable to that of group 4 until day 7; on the other hand, tumor growth was explicitly found after day 11, although the effect of tumor growth suppression was consistently better than that of group 8 after day 7. The difference in therapeutic efficacy between 5-FU treatment and 5-FC/CD@PICsome co-treatment is probably attributed to the gradual deactivation of CD after day 7. PICsome-based EPT can provide much safer treatment than treatment using 5-FU alone, that is, a higher therapeutic effect is expected for the lower dose of 5-FC and lower toxicity for the higher dose, although the dose of CD, the administration schedule, and dose of 5-FC should be optimized in the future.

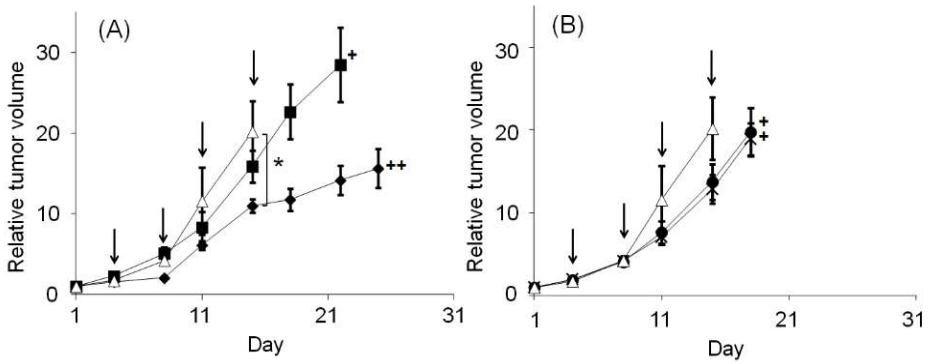

Figure III-11. Tumor growth in mice (n=5) treated with CD@PICsome and 10 mg/kg of 5-FC (A: ◆, group 1), 10 mg/kg of 5-FU (A: ■, group 3), 10 mM PBS (pH 6.8) (A and B: Δ, group 8), CD@PICsome alone (×, group 5) and 10 mg/kg of 5-FC (B: ●, group 6). An arrow indicates administration day of 5-FU or 5-FC or 10 mM PBS (pH 6.8). *: $p < 0.05$. ++: n=3,+: n=4.

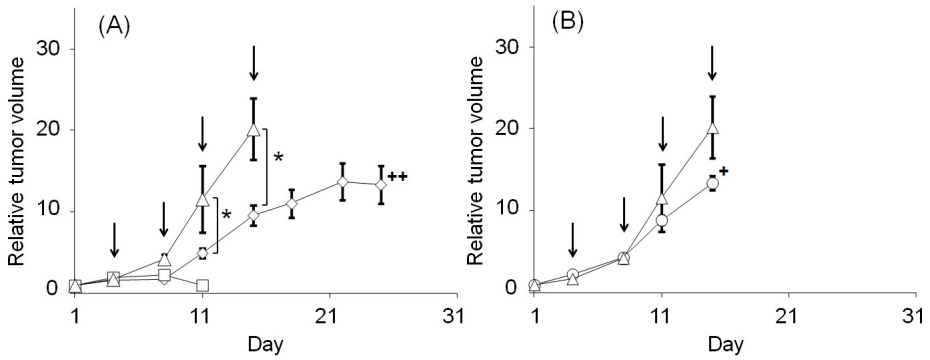

Figure III-12. Tumor growth in mice (n=5) treated with CD@PICsome and 80 mg/kg of 5-FC (A: ◊, group 2), 80 mg/kg of 5-FU (C: □, group 4), 10 mM PBS (pH 6.8) (A and B: Δ, group 8) and 80 mg/kg of 5-FC (B: ○, group 7). Arrows indicate administration day of 5-FU or 5-FC or 10 mM PBS (pH 6.8). *: $p < 0.05$. ++: n=3, +: n=4.

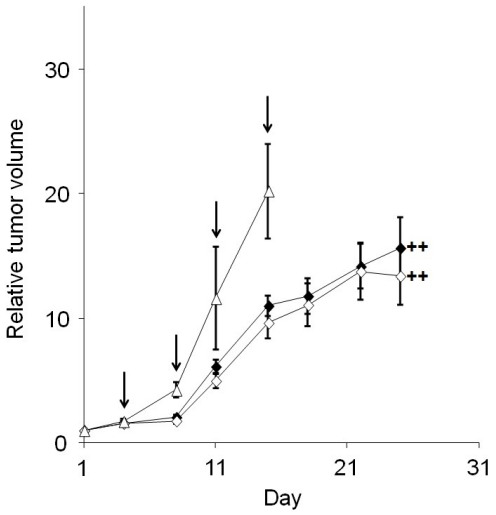

Figure III-13. Tumor growth in mice (n=5) treated with CD@PICsome and 10 mg/kg of 5-FC (◆ group 1), CD@PICsome and 80 mg/kg of 5-FC (◊, group 2), and 10 mM PBS (pH 6.8) (Δ, group 8). Arrows indicate administration day of 5-FU or 5-FC or 10 mM PBS (pH 6.8). ++: n=3.

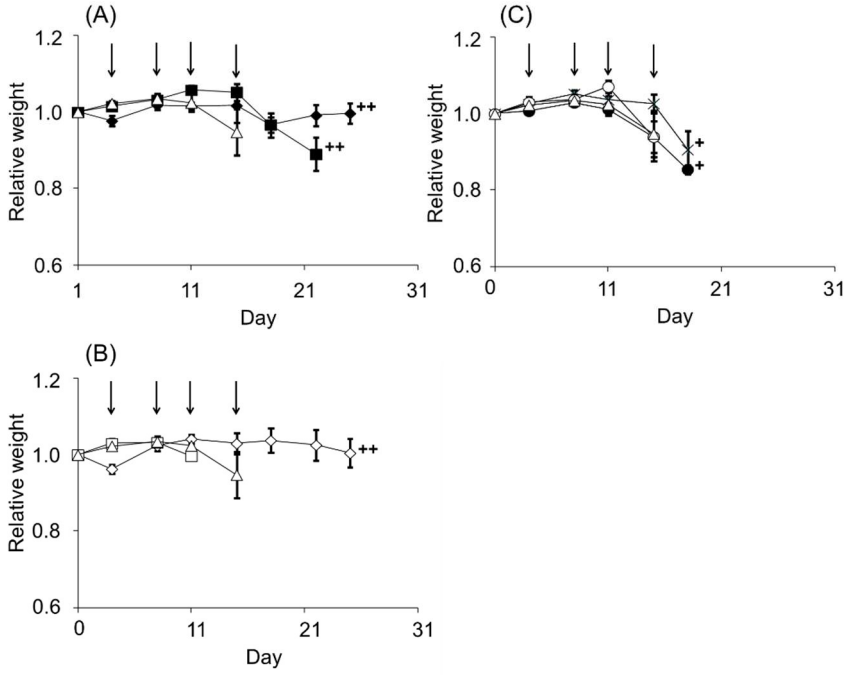

Figure III-14. The weight change of mice (n=5) treated with CD@PICsome and 10 mg/kg of 5-FC (A:◆, group 1), 10 mg/kg of 5-FU (A: ■, group 3), 10 mM PBS (pH6.8) (A, B, C: Δ, group 8), CD@PICsome and 80 mg/kg of 5-FC (B: ◊, group 2), 80 mg/kg of 5-FU (B: □, group 4), CD@PICsome alone (C: ×, group 5), 10 mg/kg of 5-FC (C: ●, group 6) and 80 mg/kg of 5-FC (C: ○, group 7). An arrow indicates administration day of 5-FC or 10 mM PBS (pH6.8). ++: n=3.

III.4. Conclusion

The SWCL method was developed to improve the encapsulation efficacy of water-soluble macromolecules such as enzymes. Water-soluble macromolecules can be encapsulated using the SWCL method, even in solutions with high ionic strength or a high concentration of charged particles. It is noteworthy that water-soluble macromolecules can be encapsulated in PICsomes of a specific size because the PICsome size is not altered during the encapsulation process, even at higher polymer concentrations, which contributes to the potential of PICsomes as a DDS. However, the dramatic improvement in the fLE value is likely due to the interaction between CD and the PIC membrane, and further studies are needed to improve fLE with other enzymes. In addition, water-soluble macromolecules, such as enzymes, that can be encapsulated have a limited molecular weight.

CD@PICsomes prepared using CD as a model enzyme were more stable for repeated use and storage than CD alone *in vitro*. Furthermore, the EPT of CD@PICsomes and 5-FC showed excellent *in vivo* antitumor effects and reduced side effects in C26-bearing carcinoma mice. CD@PICsomes and 5-FC therapy may be more effective if performed under optimal conditions; however, the dosage and administration schedule were not optimized in this study.

SWCL has the potential to encapsulate multiple enzymes in a single PICsome. This may contribute to prodrug combination therapy based on tandem enzyme reactions in PICsomes and novel prodrug designs. Thus, I believe that PICsome-based EPT can be applied to treat various diseases, including cancer, and may provide new possibilities for drug therapy.

III.5. References

III-1. Anraku, Y.; Kishimura, A.; Kamiya, M.; Tanaka, S.; Nomoto, T.; Toh, K.; Matsumoto, Y.; Fukushima, S.; Sueyoshi, D.; Kano, M.R.; et al. *Angew. Chem. Int. Ed.* **2016**, 55, 560–565.

III-2. Tang, H.; Sakamura, Y.; Mori, T.; Katayama, Y.; Kishimura, *Macromol. Biosci*. **2017**, 17, 1600542.

III-3. Anraku, Y.; Kishimura, A.; Kobayashi, A.; Oba, M.; Kataoka, K. *Chem. Commun*. **2011**, 47, 6054–6056.

III-4. Chuanoi, S.; Anraku, Y.; Hori, M.; Kishimura, A.; Kataoka, K. *Biomacromolecules*. **2014**, 15, 2389–2397.

III-5. Naoyama, K.; Mori, T.; Katayama, Y.; Kishimura, A. *Macromol. Rapid Commun*. **2016**, 37, 1087–1093.

III-6. Mutaf, O.F.; Anraku, Y.; Kishimura, A.; Kataoka, K. *Polymer*. **2017**, 133, 1–7.

III-7. Hori, M.; Cabral, H.; Toh, K.; Kishimura, A.; Kataoka, K. *Biomacromolecules*. **2018**, 19, 4113–4121.

III-8. Austin, E.A.; Huber, B.E. *Mol. Pharmacol*. **1993**, 43, 380–387.

III-9. Cheung, W.Y.; Fralick, R.A.; Cheng, S. *Curr. Oncol*. **2008**, 15, 234–236.

III-10. Phillips, T.A.; Howell, A.; Grieve, R.J.; Welling, P.G. *J. Pharm. Sci*. **1980**, 69, 1428–1431.

III-11. Vermes, A.; Guchelaar, H.-J.; Dankert, J. *J. Antimicrob. Chemother*. **2000**, 46, 171–179.

III-12. Anraku, Y.; Kishimura, A.; Oba, M.; Yamasaki, Y.; Kataoka, K. *J. Am. Chem. Soc.* **2010**, 132, 1631–1636.

III-13. Kishimura, A.; Koide, A.; Osada, K.; Yamasaki, Y.; Kataoka, K. Encapsulation of myoglobin in PEGylated polyion complex vesicles made from a pair of oppositely charged block ionomers: A physiologically available oxygen carrier. *Angew. Chem. Int. Ed.* **2007**, 46, 6085–6088.

III-14. Anraku, Y.; Kishimura, A.; Yamasaki, Y.; Kataoka, K. *J. Am. Chem. Soc*. **2013**, 135, 1423–1429.

III-15. Smith, M.J.; Haidar, I.A.; Striegel, A.M. *Analyst*. **2007**, 132, 455–460.

III-16. Sueyoshi, D.; Anraku, Y.; Komatsu, T.; Urano, Y.; Kataoka, K. *Biomacromolecules*. **2017**, 18, 1189–1196.

III-17. Malet-Martino, M.; Gilard, V.; Desmoulin, F.; Martino, R. *Clin. Chim. Acta.* **2006**, 366, 61–73.

III-18. Goto, A.; Yen, H.-C.; Anraku, Y.; Fukushima, S.; Lai, P.-S.; Kato, M.; Kishimura, A.; Kataoka, K. *ACS Biomater. Sci. Eng*. **2017**, 3, 807–815.

Chapter IV. Application of SWCL method for HPMC-encapsulated PICsome

IV.1. Introduction

As described in I.2.4, PICsome cannot retain water-soluble low molecular-weight compounds (WLMWCs) because PICsome is a vesicle composed of a semipermeable membrane. To overcome this issue, I attempted to improve the retention and sustained release of WLMWCs by encapsulating a water-soluble polymer that shows viscosity when dissolved in water in the inner aqueous phase of PICsome.

Hydroxypropyl methylcellulose (HPMC) is selected as a viscosity enhancer for the inner water phase of PICsomes. In the pharmaceutical field, HPMC is widely used for oral solid formulations as a sustained-release matrix, binder, coating base material, and solid dispersion base material [IV-1,IV-2]. The viscosity of the HPMC solution can vary depending on its concentration, degree of polymerization, and degree of substitution by the methyl and hydroxypropyl moieties [IV-2]. HPMC with molecular weights ranging from tens of thousands to millions are available. Thus, it is easy to select one that can pass through the PIC membrane. In this study, I developed PICsomes that encapsulated a viscosity-enhanced liquid matrix in the inner cavity for the sustained release of WLMWCs. This new formulation was fabricated based on a SWCL method that allowed the encapsulation of HPMC in the inner water phase of PICsomes to form HPMC-encapsulated PICsomes (HPMC@PICsomes, Figure IV-1). In this study, the SWCL method was slightly modified to encapsulate HPMC into PICsomes. As described in chapter III, pCL-PICsomes were prepared by treatment with 1 equivalent for the crosslinking agent, 1-ethyl-3-(3-dimethylaminopropyl)carbodiimide hydrochloride (EDC). Subsequently, the pCL-PICsomes were exposed to HPMC solution under sonication for encapsulation via passive diffusion for different treatment periods. Two types of HPMC with different degrees of polymerization were selected: TC-5R (M_w:35,600, M_w/M_n:1.62) and 60SH-50 (M_w:76,800, M_w/M_n:2.64). Typically, a difference in the degree of polymerization leads to a difference in viscosity when dissolved in water. The TC-5R and 60SH-50 solutions were prepared at the highest concentrations at which solvation was not time-consuming (10% TC-5R and 5% 60SH-50). The HPMC-encapsulated PICsome (HPMC@PICsome) prepared in this way was evaluated for its retain and release ability of model WLMWCs such as water-soluble dye and drug.

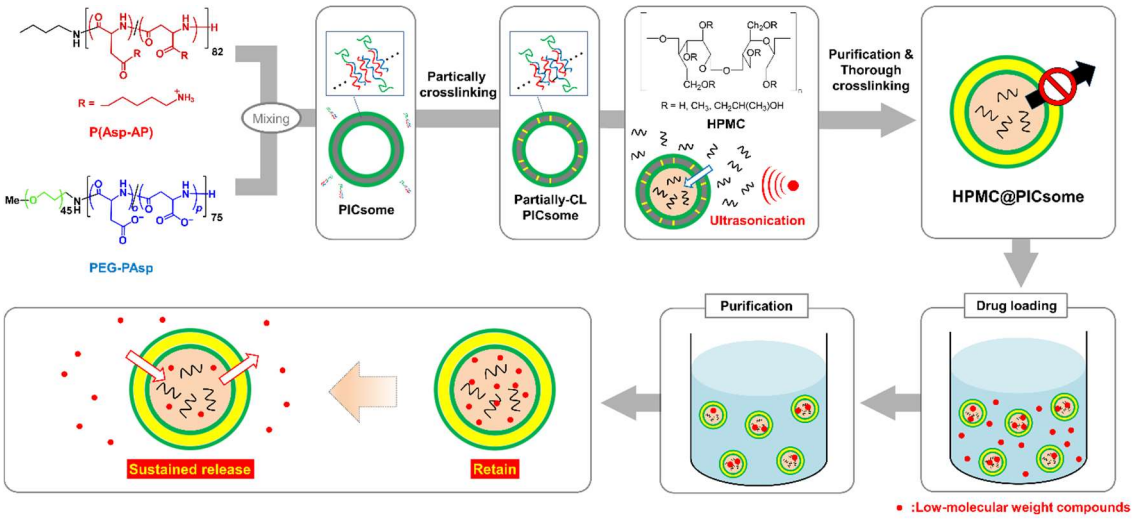

Figure IV-1 The schematic illustration of the fabrication flow of HPMC@PICsome, prepared using the modified SWCL method.

IV.2. Material and Methods

IV.2.1. Materials

Poly(5-aminopentyl-α,β-aspartamide) (P(Asp-AP), with a degree of polymerization (DP) of 82) and polyethylene glycol (PEG)-block-poly(α,β-aspartic acid) (PEG-PAsp, DP of PAsp = 75; Mn of PEG = 2,000, Mw/Mn of PEG = 1.05), were synthesized as reported previously [IV-3]. 1-Ethyl-3-(3-dimethylaminopropyl) carbodiimide hydrochloride (EDC) was purchased from Dojindo Molecular Technologies, Inc (Kumamoto, Japan). Hydroxypropyl methylcelluloses (HPMCs), TC-5R® and Metrose® 60SH-50, were purchased from Shin-Etsu Chemical Co., Ltd (Tokyo, Japan). Rose Bengal (RB) was purchased from Wako Pure Chemical Industries, Ltd (Osaka, Japan). Gemcitabine (GEM) was purchased from Tokyo Chemical Industry Co., Ltd (Tokyo, Japan). All reagents were used without further purification.

IV.2.2. Material characterization

Particle size distribution was measured by dynamic light scattering (DLS) using Zetasizer-nano (Malvern Instruments Ltd., Worcestershire, UK). Transmission electron micrographs (TEM) were obtained using a JEM-1400 transmission electron microscope (JEOL Ltd., Tokyo, Japan) operating at 120 kV. The samples for TEM observation were dispersed in ultrapure water, and transferred onto copper grids (400 mesh size; coated with a thin film of collodion and carbon), followed by staining with uranyl acetate. UV-visible spectra were obtained on a Nanodrop ND-1000 (Thermo Fisher Scientific Inc.). HPMC release test was performed by size exclusion chromatography (SEC) equipped with a reflective index detector. The measurement of u-PIC ratio was performed by

size exclusion chromatography (SEC) equipped with a fluorescence detector. Loading and release behaviors of RB and GEM were evaluated by SEC equipped with a UV-visible detector monitored at the fixed wavelength of 270 nm for GEM and 550 nm for RB. A Superdex 200 column 10/300 GL (Cytiva, Marlborough, MA, USA) was used for the separation of PICsome and low molecular weight compounds.

IV.2.3. Preparation method of HPMC-encapsulated PICsome (HPMC@PICsome)

Typically, P(Asp-AP) and PEG-PAsp were separately dissolved in 10 mM phosphate buffer (PB; pH7.4) at a concentration of 1.0 mg/mL. Then, 40 μL of the P(Asp-AP) solution and 48 μL of the PEG-PAsp solution were mixed by 2-min vortexing to contain the same mole of $–NH3^+$ from P(Asp-AP) and $–COO^–$ from PEG-PAsp. Next, 50 μL of 1.0 mg/mL EDC solution was added to the reaction mixture and stood overnight at room temperature to crosslink the PIC layer. The resulting solution was purified using a polyethersulfone (PES) ultrafiltration membrane Vivaspin 6 (molecular weight cut-off (MWCO): 300,000, Sartorius, Göttingen, Germany) at 25 °C. The medium exchange was repeated 10 times to completely remove byproducts to obtain the partially-crosslinked PICsome (pCL-PICsome).

Twenty microliters of pCL-PICsome solution (polymer concentration: ca. 20 mg/mL) were dropped into 0.5 mL of X% HPMC solution (X = 10 for TC-5R; 5 for 60SH-50), the mixed solution was ultrasonicated at 20 kHz and 120 V for 5 min using VP-30S (TAITEC CORPORATION, Japan). Subsequently, for further crosslinking of the PIC layer, 0.5 mL of 10 mg/mL ECD solution was added to the pCL-PICsome solution, and stood overnight at room temperature. After overnight incubation, the sample was diluted with ultrapure water to the concentration of loaded HPMC ≤ 0.1%. Then, the resulting solution was purified using a PES ultrafiltration membrane Vivaspin 6 (MWCO: 300,000, Sartorius) at 25 °C. The medium exchange was repeated 10 times to completely remove byproducts to obtain the TC-5R-encapsulated PICsome and 60SH-50-encapsulated PICsome (TC-5R@PICsome and 60SH-50@PICsome, respectively).

To calculate the u-PIC, Cy5-labeled pCL-PICsomes (Cy5-pCL-PICsomes) were prepared using Cy5-conjugated PEG-PAsp (PEG-PAsp-Cy5) instead of non-labeled PEG-PAsp, as previously reported [IV-4]. The amount of u-PIC was determined by SEC by monitoring the fluorescence (Em/Ex = 650/670 nm) of Cy5-labeled PEG-PAsp.

IV.2.4. Loading and release profile

For loading model compounds of WLMWC, RB and GEM, a hundred microliter of TC-5R@PICsome solution with a total polymer concentration of 20 mg/mL was added to 5.0 mL of 10 mg/mL RB solution or 10 mg/mL of GEM solution, and stood for overnight at room temperature. The resulting solution was purified using a PES ultrafiltration membrane Vivaspin 6 (MWCO: 300,000, Sartorius) at 25 °C. The medium exchange was repeated 10 times to completely remove excess RB or GEM from the solution to obtain the RB-loaded TC-5R@PICsome (RB-TC-5R@PICsome) and GEM-loaded TC-5R@PICsome (GEM-TC-5R@PICsome). RB-loaded 60SH-50@PICsome (RB-60SH-50@PICsome) and GEM-loaded 60SH-50@PICsome (GEM-60SH-50@PICsome) were prepared using the same procedure using 60SH-50@PICsome instead of TC-5R@PICsome. Loading amount was calculated from the concentration change of a model compound before and after loading, which was determined by SEC analysis of unpurified WLMWC-loaded HPMC@PICsome.

For the release test, each HPMC@PICsome was prepared using 10 mM phosphate-buffered saline (PBS; 10 mM PB with 150 mM NaCl, pH7.4) at 5.0 mg/mL of total polymer concentration, and 2.0 mL of the solution was placed into a dialysis bag. The outer solution was monitored at 37 °C using 20 mL of 10 mM PBS (pH7.4) as an outer solution. The release amounts of RB and GEM were evaluated by SEC at the designated time point.

IV.3. Results and discussion

IV.3.1. Preparation of crosslinked PICsomes loaded with HPMC (HPMC@PICsomes) by SWCL method

Unpurified pCL-PICsome was measured by SEC to calculate the amount of the charged polymers that did not participate in the PICsome formation (uPIC) (Figure IV-2). The peak (a) is assigned to the pCL-PICsome, and the peak (b) is assigned to the uPIC. The ratio of uPIC was calculated by the following equation:

$$\text{The ratio of u-PIC (\%)} = \frac{\text{Peak area of (b)}}{\text{Peak area of (a)} + \text{(b)}} \times 100$$

From this measurement, it was calculated that 32% of polymers was existed as uPIC.

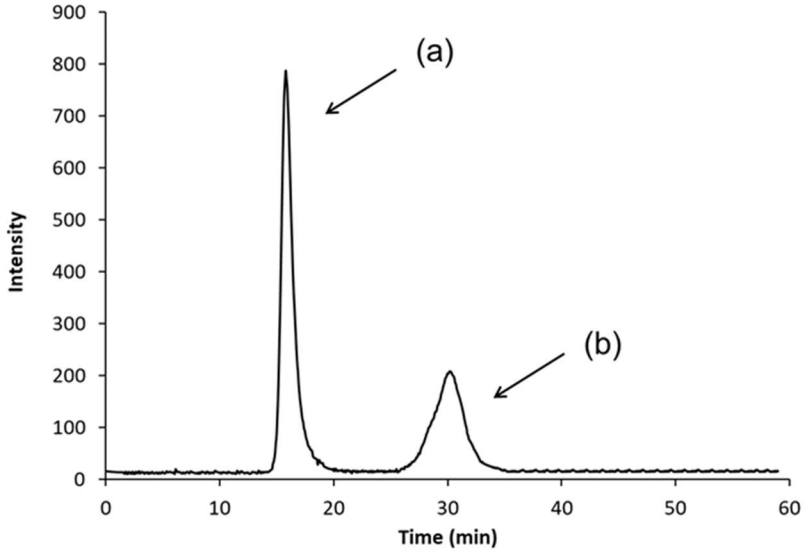

Figure IV-2 SEC chromatogram of pCL-PICsome before purification.

Next, the effect of sonication time for the SWCL method was examined. pCL-PICsome was added to the HPMC solution as same procedure described in section IV.2.3, then HPMC@PICsome was prepared with different sonication times of 1, 5, and 10 min at 20 kHz and 120 V output. The particle size distribution of resulted PICsomes were shown in Table IV-1. Although sonication for 10 min resulted in the formation of precipitates, short-term treatments and 1- and 5-min treatments resulted in well-dispersed particles. TEM images of HPMC@PICsomes obtained after 1- and 5-min sonication showed no significant differences (Figure IV-3 and Figure IV-4). In subsequent experiments, HPMC@PICsomes prepared via 5-min sonication were used.

Table IV-1 Size and polydispersity index (PDI) of the resulting HPMC@PICsomes.

Sample	Loading compound	Sonication time (min)*1	Size (nm)	PDI
pCL-PICsomes	-	-	99	0.087
10% TC-5R @PICsomes	-	1	117	0.124
	-	5	117	0.147
	RB	5	117	0.124
	GEM	5	114	0.151
5% 60SH-50 @PICsomes	-	1	114	0.115
	-	5	114	0.129
	RB	5	113	0.146
	GEM	5	112	0.134

*1: Sonication time for the preparation of HPMC@PICsomes, not for loading of RB or GEM.

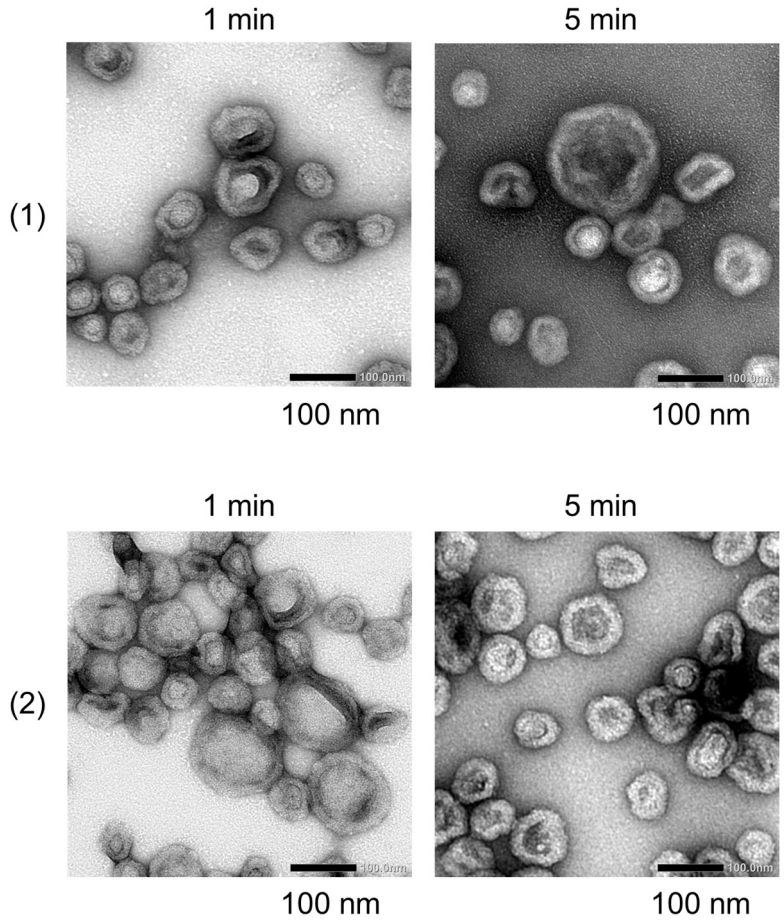

Figure IV-3 TEM images of HPMC@PICsome. (1) 10% TC-5R@PICsome and (2) 5% 60SH-50@PICsome after 1- and 5-min sonication for encapsulating HPMC.

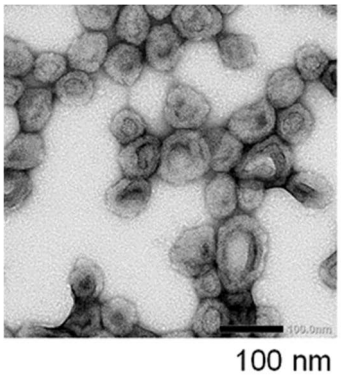

Figure IV-4 TEM images of pCL-PICsome.

IV.3.2. Stability of HPMC@PICsome

To evaluate the stability of HPMC@PICsomes, the leaching of HPMC from HPMC@PICsomes was measured using SEC. For both HPMC@PICsomes, leaching of HPMC was not confirmed 48 h after preparation (Figure IV-5 and Figure IV-6). Therefore, HPMC@PICsomes stably encapsulated HPMC for at least 48 h after the second crosslinking step. In addition, the colloidal stability of HPMC@PICsomes was evaluated using DLS in 10 mM phosphate-buffered saline (PBS; 10 mM PB with 150 mM NaCl, pH 7.4; Figure IV-7). No significant size changes were observed for both HPMC@PICsomes for 24 h, indicating their appropriate stability under subsequent experimental conditions.

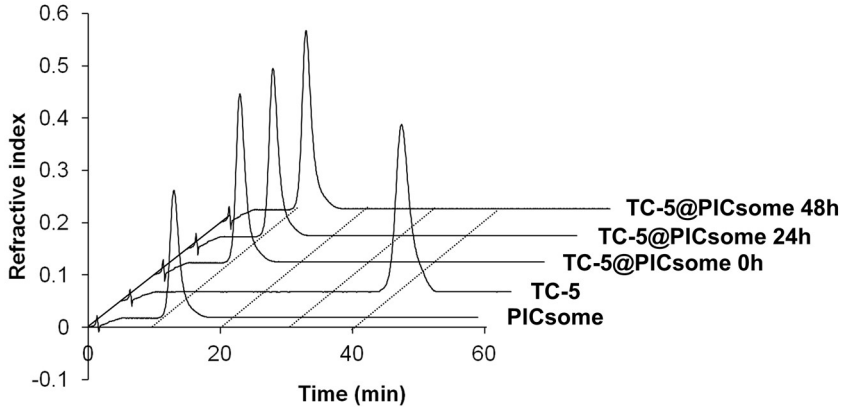

Figure IV-5 HPMC retention behavior of TC-5R@PICsome**.**

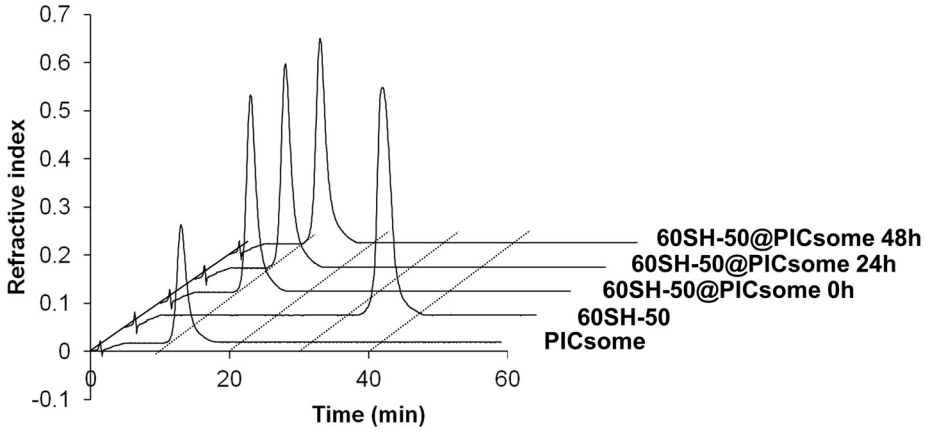

Figure IV-6 HPMC retention behavior of 60SH-50@PICsome.

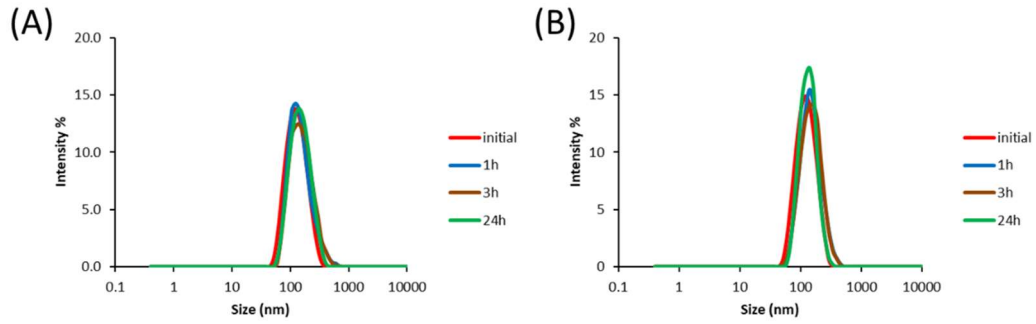

Figure IV-7 Time-dependent change in size distributions of TC-5R@PICsome (A) and 60SH-50@PICsome (B) evaluated by DLS.

IV.3.3. Loading and release profile

The loading of drugs onto the HPMC@PICsomes was investigated using the model compounds, rose bengal (RB) and gemcitabine (GEM). The loading of RB and GEM was performed in a mixed solution with final concentrations of 0.39 mg/mL PICsomes and 9.8 mg/mL RB or GEM (Figure IV-1). The loading amount was calculated from the difference between the initial and residual concentrations of free RB or GEM, as determined via SEC using an unpurified reaction mixture. The loading amount of the model compound was defined as the ratio of the total polymer amount of the PICsomes and was calculated using the following equation:

$$\text{Loading amount (\%)} = \frac{(C_1 - C_2)V}{W_P - W_U} \times 100$$

C_1: Initial concentration of a model compound (mg/mL)

C_2: Concentration of the free model compound in sample (mg/mL)

V: Unpurified sample volume (mL)

W_p: A feed amount of the polymer for PICsome formation (mg)

W_u: The calculated amount of the charged polymers not participating in PICsome formation (mg)

The loading amounts of RB and GEM were 2% for TC-5R@PICsome and 4% for 60SH-50@PICsome. However, on performing the same operation using PICsomes without HPMC, neither RB nor GEM was retained in the PICsomes. These results suggest that the PIC membrane cannot entrap WLMWCs. Notably, a negligible difference was observed in the size of each HPMC@PICsome before and after the loading of RB and GEM (Table IV-2).

Table IV-2 Size and PDI of the resulting HPMC@PICsomes after loading model compounds.

Sample	Loading compounds	Loading Amount (%)	Size (nm)	PDI
pCL-PICsomes	-	-	99	0.087
10% TC-5R@PICsomes	-	-	117	0.147
	RB	2	117	0.124
	GEM	2	114	0.151
5% 60SH-50@PICsomes	-	-	114	0.129
	RB	4	113	0.146
	GEM	4	112	0.134

RB and GEM release profiles were obtained via SEC after the removal of the unencapsulated drug (Figure IV-8). All drug-loaded HPMC@PICsomes showed more than 60% release in 24 h, and almost 100% of RB and GEM were released after 96 h. These results indicate that WLMWCs were successfully loaded and released in a sustained manner. Each profile was fitted to first-order release kinetics (Figure IV-9). For 60SH-50@PICsomes, the correlation coefficient of the approximate curves calculated from 4 data from the initial to 96 h was as low as 0.7401. When the 96 h data was removed, the correlation coefficient improved to 0.8153. Probably, 60SH-50@PICsome showed faster release, which would provide an insufficient amount of data for curve fitting. Although the viscosity of the TC-5R solution was significantly different from that of the 60SH-50 solution, the HPMC@PICsomes showed almost the same loading amount and release profile, regardless of the polarity of the WLMWCs. Since HPMC does not possess a charged moiety, loading and release behaviors would not be regulated by electrostatic interaction. Presumably, sustained releases are achieved by a highly viscous matrix with high polarity. A polymersome encapsulating a temperature-responsive polymer named Hydrosomes (Hs) were reported previously [IV-5]. Hs show a sustained-release profile but involve an initial burst; this initial burst can be explained by the property of the encapsulated polymer, which can interact with the polymersome membrane to cause membrane destabilization. The suppressed initial burst of WLMWCs from HPMC@PICsomes compared to Hs suggest that HPMC is mainly filled in the inner cavity of HPMC@PICsome and that the membrane of PICsome is more stable than that of polymersomes. Another analogous example is gel-in-liposome (GiL) [IV-6]. The internal aqueous phase of the liposome is gelated to improve the mechanical resistance against chemical stress. According to GiL results, WLMWCs release behavior is completely controlled by the membrane property; however, in the case of HPMC@PICsome, the release behavior is governed by not the membrane but the HPMC because the PIC membrane always shows high permeability for WLMWCs.

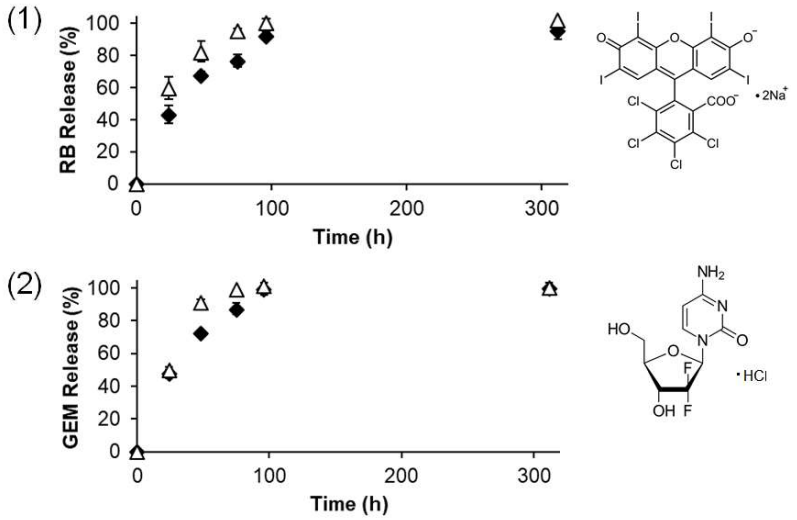

Figure IV-8 Release profiles of (1) RB and (2) GEM from HPMC@PICsome. ♦: TC-5R@PICsomes, △: 60SH-50@PICsomes. n = 3.

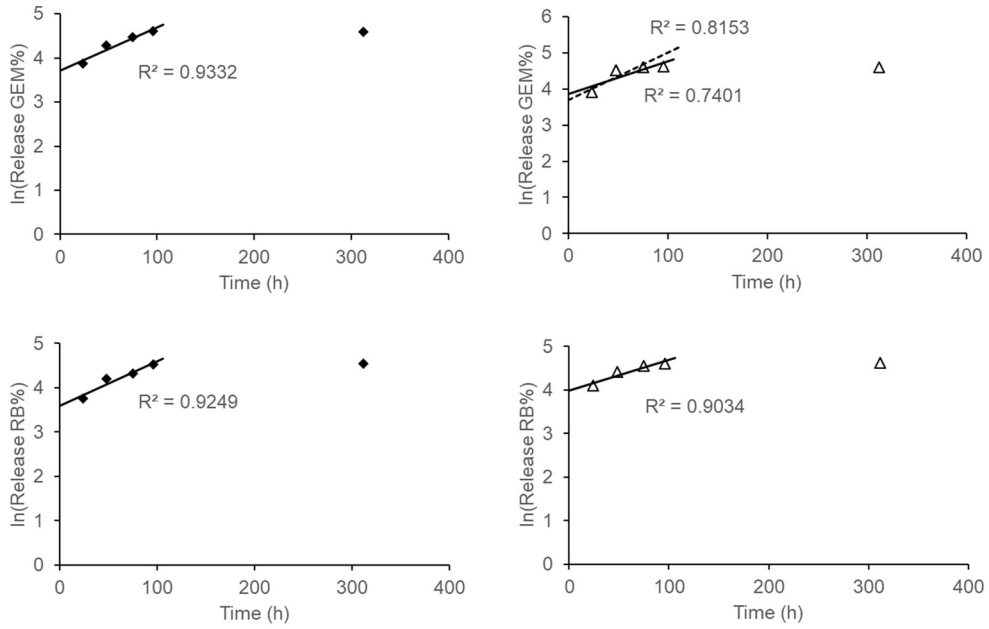

Figure IV-9 Fitting curves of GEM (top) and RB (bottom) from HPMC@PICsome. ♦: TC-5R@PICsome, △: 60SH-50@PICsome. Solid lines show the approximate curve calculated using the initial four data points. A dotted line shows the approximate curve calculated using the initial three data points.

To determine the effect of the preparation methods, TC-5R@PICsomes were prepared by vortex mixing or without agitation (standing), instead of sonication. The results obtained using 3 hours vortex mixing and 2 days standing showed the same loading amounts for both RB and GEM compared to those obtained using sonication for 5 min. This result indicates that the TC-5R concentration in the vesicle inner phase was similar in all cases. Therefore, sonication can accelerate the loading of TC-5R most effectively in terms of treatment time. Regardless of the preparation method, the size and PDI of the TC-5R@PICsomes were not significantly different from those of the pCL-PICsomes (Table IV-3).

Table IV-3 Loading behaviors of TC-5R@PICsomes for different loading methods

Sample	HPMC-loading method	RB (%)	GEM (%)	Size (nm)	PDI
pCL-PICsome	-	ND	ND	99	0.087
TC-5R @PICsome	Standing, 1 d	0	0	101	0.104
	Standing, 2 d	1	1	111	0.116
	Vortex mixing, 1 h	0	0	113	0.121
	Vortex mixing, 3 h	1	1	105	0.115

ND: not detected

IV.4. Conclusion

In this study, HPMC@PICsome was successfully prepared as a WLMWC reservoir by encapsulating HPMC into PICsome. It takes a long time for encapsulation of HPMC if the SWCL method developed in Chapter III is used, due to viscous HPMC solution. However, it was found that SWCL method with the ultrasonication instead of the vortex mixing could save time for encapsulation process. HPMC@PICsomes showed primary release behavior by retaining model WLMWCs, which was not possible with normal PICsomes. Since HPMC cannot permeate the PIC membrane after the second crosslinking, the inner cavity of HPMC@PICsomes are expected to be viscous just after encapsulation of HPMC. Therefore, the amount of HPMC loaded into HPMC@PICsomes correlates well with the sustained release performance. HPMC@PICsomes are promising as DDS nanocarriers, taking advantage of PICsomes, the excellent blood circulation and tumor accumulation. However, further studies are required on the relationship between encapsulation amount of HPMC and the sustained release ability of WLMWC.

IV.5. References

IV-1. J. E. Hogan, *Drug Dev. Ind. Pharm*. **1989**, 15, 975.

IV-2. M. M. Al-Tabakha, *J. Pharm. Pharm. Sci*. **2010**, 13, 428

IV-3. Anraku, Y.; Kishimura, A.; Oba, M.; Yamasaki, Y.; Kataoka, K. *J. Am. Chem. Soc*. **2010**, 132, 1631−1636.

IV-4. Kishimura, A.; Koide, A.; Osada, K.; Yamasaki, Y.; Kataoka, K. Encapsulation of myoglobin in PEGylated polyion complex vesicles made from a pair of oppositely charged block ionomers: A physiologically available oxygen carrier. *Angew. Chem. Int. Ed.* **2007**, 46, 6085–6088.

IV-5. J. S. Lee, W. Zhou, F. Meng, D. Zhang, C. Otto and J. Feijen. Thermosensitive hydrogel-containing polymersomes for controlled drug delivery. *J. Control. Release*. **2010**, 146, 400–408.

IV-6. S. Petralito, R. Spera, S. Pacelli, M. Relucenti, G. Familiari, A. Vitalone, P. Paolicelli, M. A. Casadei. Design and development of PEG-DMA gel-in-liposomes as a new tool for drug delivery. *React. Funct. Polym*. **2014**, 77, 30–38.

Chapter V. Conclusion and future perspective

V.1. General conclusion

The aim of this study was increasing the value of PICsome as the DDS platform by the development of new water-soluble macromolecules encapsulation method for PICsome (SWCL method). This SWCL method enhance the feed-to-loading efficacy, resulted PICsome enabled retaining/sustained release of WLMWCs and PICsome-based EPT.

In Chapter II, MSN@PICsome enabled to deliver WLMWCs to tumor. The retaining of WLMCs was impossible using normal PICsome. Moreover, I found that surface modification of the encapsulated MSN was possible even after preparation of MSN@PICsome to accommodate more drugs. However, the amount of encapsulated MSN has not been optimized, and further studies are needed for efficiently use. Furthermore, although the encapsulation ratio of fed MSN was improved, it would be necessary to consider reducing the ratio of empty PICsomes. Alternatively, if we exclude cost and production efficiency and focus only on WLMWCs delivery, empty PICsomes without WLMWCs delivery capability should be removed in the purification process.

In Chapter III, I developed a new method for encapsulation of water-soluble macromolecules, the SWCL method, and successfully encapsulated the enzyme into PICsome under higher salt/polymer/enzyme concentration condition. The obtained CD@PICsomes showed higher enzyme activity, suggesting that encapsulated amount of enzymes was increased than the conventional method. Increasing the enzyme activity of CD@PICsome enabled to apply to *in vivo* EPT in mice. In other word, the basis for DDS which work as an *in vivo* nanoreactor has been completed. In addition, encapsulated CD was protected by PIC membrane, resulting that improved stability is advantage for storage. However, the high encapsulation efficacy would be due to the interaction between CD and the PIC membrane, further study is required about the encapsulation efficacy using other enzymes by SWCL method. It is important to note that the molecular weight of the enzyme that can be encapsulated by the SWCL method is limited, enzymes that can be applied to the SWCL method is also issue for future study. Furthermore, from the viewpoint of PICsome-based EPT, the dosage and schedule of CD@PICsome and 5-FC may be optimized for effective therapy.

In Chapter IV, I applied the SWCL method to encapsulate water-soluble polymer in viscous solution. Obtained HPMC@PICsome showed sustained-release of WLMWCs, and exhibits primary release behavior. Although HPMC@PICsome is in the basic research stage of use testing, it was shown to add functionality to PICsome as my hypothesized. However, many issues remain to be addressed. The relationship between encapsulation amount of HPMC and the sustained release ability of WLMWCs (improvement of WLMWC loading amount, and optimization of loading and sustained release of WLMWC), *in vivo* data (biodistribution and its ability to retain/release drugs *in vivo*) are essential.

In this study, I investigated the application of PICsome in three different ways, and found that it was possible to prepare new functionalized PICsomes without significantly change of its properties

in any of the applications. In other words, PICsome has a potential as a DDS platform that can be used for various applications, and I succeed to testify that possibilities of PICsome for the future.

V.2. Future perspective

The developing of SWCL method is the most valuable finding in this study.

The SWCL method, a new encapsulation method utilizing the characteristics of PICsome, can be applied not only for polymers but also for enzymes, and dramatically improve the previously low encapsulation efficacy. Improvement of PICsome function allow for the application of the PICsome to new therapeutic modalities. Although this is a feasibility study of EPT application, I believe that the demonstration of *in vivo* therapy in PICsome-based EPT will lead to the next step for social implementation. However, there are many points to be optimized for PICsome-based EPT in the 5-FC/CD system, including the preparation method (encapsulation amount of enzyme), PICsome size, administration dose (both of CD@PICsome and 5-FC) and schedule, and so on. In other words, further optimization of this system may lead to more effective EPT. Furthermore, it is theoretically possible to encapsulate multiple enzymes, which would applied various applications. For the next step of PICsome-based EPT, it is necessary to demonstrate that the SWCL method can be applied to many enzymes, not just CD. I should be pay attention to the possibility that fLE of CD would be exceptionally high due to its interaction with the PIC membrane. To confirm this note, SWCL method using other enzymes should be performed. Very recently, other enzyme-encapsulated PICsome, methionine γ-lyase encapsulated PICsome have been reported. The particle characteristics of methionine γ-lyase encapsulated PICsome are analyzed, however, the pharmacokinetics has not been reported yet [V-1,V-2]. Thus, PICsome-based EPT is certainly developing and approaching social implementation.

It was possible to change the internal properties of PICsome by using the SWCL method, and it was also possible to encapsulate nano-sized inorganic adsorbents by changing the order of mixing. These methods made it possible to retain and sustained release of WLMWCs, which was not possible in the past. Another advantage of PICsome is that encapsulated MSN can be modified its surface to change its physical properties. However, since these findings are still in the feasibility study stage, there are many issues, such as improving loading amount, controlling sustained release, and optimizing the dose. One idea is that PICsome encapsulated polymers which behave gel below body temperature may enable control of sustained release in the body. If I use the polymer which transform sol to gel under body temperature (assuming 30°C), the inner aqueous phase of PICsome is a sol below 30°C, the concentration of drugs in both inner and outer of PICsome is equilibrate as at storage. While, when this PICsome solution is warmed over 30°C before administration, drug is retained in PICsome and released in sustained manner after administration. Another idea is that the photodegradable polymer that gels when dissolved in water encapsulated PICsome may enable preparation of

formulations that release drugs topically triggered by external stimuli. The PICsome can be applied for local therapy, drugs are released only where externally stimulated.

From such feasibility studies, it might be possible to use the drug which have a strong side effects or insufficiently effective. In other words, PICsome can contribute to the aim of DDS formulation, which is to reduce side effects and maximize drug efficacy. Furthermore, in the case of EPT, PICsome has the potential to work as a nanomachine that removes and treats abnormalities in the body until loss of enzyme activity. In addition, there are reports about active targeting of PICsome by ligand modification [V-3] and application as an imaging agent [V-4]. I believe that the establishment and combination of each of these technologies will enhance the value of PICsome as a DDS Platform. I believe that the establishment and combination of each of these technologies will enhance the value of the PICsome as a DDS Platform.

V.3. References

V-1. Vasily Koval, Elena Morozova, Svetlana Revtovich, Anna Lyfenko, Arpi Chobanian, Viktoria Timofeeva, Anna Solovieva, Natalya Anufrieva, Vitalia Kulikova, and Tatyana Demidkina. Characteristics and Stability Assessment of Therapeutic Methionine γ-lyase-Loaded Polyionic Vesicles. *ACS Omega* **2022**, 7, 959−967.

V-2. E. Morozova, V. Koval, S. Revtovich, A. Lyfenko, A. Minakov, A. Chernov, G. Telegin, D. Kirilenko, A. Chobanian, N. Anufrieva, V. Kulikova, T. Demidkina. Phytoestrogens decorated nanocapsules for therapeutic methionine γ-lyase targeted delivery. *Biochimie* **2023**, 209, 1−9.

V-3. Wataru Kawamura, Yutaka Miura, Daisuke Kokuryo, Kazuko Toh, Naoki Yamada, Takahiro Nomoto, Yu Matsumoto, Daiki Sueyoshi, Xueying Liu, Ichio Aoki, Mitsunobu R Kano, Nobuhiro Nishiyama, Tsuneo Saga, Akihiro Kishimura, Kazunori Kataoka. Density-tunable conjugation of cyclic RGD ligands with polyion complex vesicles for the neovascular imaging of orthotopic glioblastomas. *Sci. Technol. Adv. Mater*. **2015**, 16, 035004.

V-4. Daisuke Kokuryo, Yasutaka Anraku, Akihiro Kishimura, Sayaka Tanaka, Mitsunobu R. Kano, Jeff Kershaw, Nobuhiro Nishiyama, Tsuneo Saga, Ichio Aoki, Kazunori Kataoka. SPIO-PICsome: Development of a highly sensitive and stealth-capable MRI nano-agent for tumor detection using SPIO-loaded unilamellar polyion complex vesicles (PICsomes). *J. Controlled Release*, **2013**, 169, 220–227.

List of publications

1. Goto, A. Yen, H.-C. Anraku, Y. Fukushima, S. Lai, P.-S. Kato, M. Kishimura, A. Kataoka, K. Facile preparation of delivery platform of water-soluble low-molecular-weight drugs based on polyion complex vesicle (PICsome) encapsulating mesoporous silica nanoparticle. *ACS Biomater. Sci. Eng*. **2017**, 3, 807–815.
2. A. Goto, Y. Anraku, S. Fukushima, A. Kishimura. *Polymers* **2023**, 15, 1368.
3. A. Goto, Y. Anraku, S. Fukushima, A. Kishimura. *Chem. Lett.* 2024, 53, 5, upae070.

Acknowledgements

I thank K. Kataoka, Innovation Center of NanoMedicne, Kawasaki Institute of Industrial Promotion, for useful discussions. He always helped me with his wealth of knowledge. T.Ishii, S. Fukushima, K. Osada, Y. Yamasaki, H. Cabral, K. Miyata, Y. Anraku, N. Nishiyama and A. Kishimura also gave me helpful comments and advices. H. Hoshi supported me in the TEM measurements. And, I want to say thank many stuffs and students in Kataoka Lab for kindly help. I believe that my experience at Kataoka Lab will be an asset for me for the rest of my life, and will help my life.